Design and Fabrication of a Wide Band Meandering Antenna for X-band Applications

by

Muhammad Sohail Anwar

A Thesis Submitted to the
Graduate School of Sciences and Engineering
in Partial Fulfillment of the Requirements for
the Degree of

Master of Science

in

Optoelectronics and Photonics Engineering

Koç University

September 2015

Istanbul

Koç University
Graduate School of Sciences and Engineering

This is to certify that I have examined this copy of a master's thesis by

Muhammad Sohail Anwar

and have found that it is complete and satisfactory in all respects,
and that any and all revisions required by the final
examining committee have been made.

Committee Members:

____
Prof. Dr. Ali Serpengüzel, Ph. D. (Advisor)

____
Associate Prof. Dr. Kaan Güven, Ph. D.

____
Prof. Dr. Hilmi Ünlü, Ph. D.

Date: ____________________

ABSTRACT

Novel meandering antenna designs have been proposed for broadband communication applications in X-band spectral region. Broad band antennas are becoming more popular as a result of growing demand for bandwidth, for example, video conferencing; direct sequence spread spectrum (DSSS) communication system and frequency hopping. Meanders introduce longer current paths and hence add multiple staggered resonating modes. This design technique can be used to achieve multiband designs using resonating modes far from each other. However, if the design is engineered to let these resonant modes come closer to each other, they will complement the effect of closely spaced resonances, forming staggered resonating behavior, and broadband antennas are achieved. Current in the adjacent arms of the meandering antennas cancel out each other due to symmetry of the design, and radiation efficiency is compromised as a result. Antisymmetric meandering arms are presented in this work, to achieve higher radiation efficiency. A relationship between physical dimensions of the meandering loops, that is, height, thickness, mutual coupling and material properties are presented and resonant frequencies are mathematically modeled. The physical dimensions are selected to obtain set of resonant frequencies, which are closely spaced in the frequency spectrum. The model is simulated using finite element method (FEM) numerical modeling technique. A good agreement between mathematically calculated resonant response and simulated results is obtained for different designs geometries. Six designs are modeled and fabricated on a single sided FR4 substrate of dielectric constant 4.4 and thickness 1.6 mm. In order to evaluate the performance for suitable comparison, each antenna is identically implemented using a 50-Ohm coplanar waveguide (CPW) as feeding probe. Antennas are independently assessed using a Network Analyzer. Both S11 and S12, VSWR, efficiency, gain and bandwidth (BW) parameters are measured. The overall performance of the antennas has been found good.

ÖZET

Bu tezde, geniş dalga kıvrımlı anten tasarımları X-bant sıklıklarındaki uygulamalar için önerilmiştir. Geniş dalga antenler; görüntülü konuşma, doğrudan ardışık dağıtılmış izge (DADİ) iletişim sistemleri ve sıklık atlama gibi alanlarda giderek artan bir ilgi görmektedir. Kıvrımlı alıcılar, elektrik akımı için daha uzun akış yolu sağladığından çoklu ve birbirine eklenebilen çınlama kipi özellikleri de göstermektedir. Bu tasarım yöntemleri; birbirinden uzak çınlama kiplerini kullanarak çoklu-bant tasarımlarına yakınlaşır. Eğer hedeflenen tasarım, birbirinden uzak çınlamaları bir araya getirerek çınlama eklenmesi durumu yaratabilirse, geniş bant antenler elde edilebilir. Kıvrımlı antenlerde birbirine komşu kollarda yol alan elektrik akımları simetri nedeniyle birbirlerini yok ederek ışıma veriminde düşüşe neden olmaktadır. Bu çalışmada, daha yüksek ışıma verimi elde etmek amacıyla anti-simetrik kıvrımlı anten kolları tasarımı sunulmaktadır. Yükseklik, kalınlık, ortak bağlanma özellikleri gibi değişkenler kıvrımlı anten halkaları için hesaplanmış ve çınlama sıklıkları kuramsal yollarla ortaya konulmuştur. Bu noktada fiziksel değişkenler çınlama sıklıklarının birbirlerine yakın olması amaçlanarak seçilmiştir. Oluşturulan kuramsal model sonlu bileşenler yöntemi (SBY) sayısal tasarlama yöntemi ile benzeştirilmiştir. 6 ayrı anten tasarımı benzeşim sonuçlarına göre tasarlanmış ve dielektrik katsayısı 4.4 ve kalınlığı 1.6 mm olan tek yüzlü iletken FR4 üzerinde üretilmiştir. Anten tasarımlarının başarım ölçümleri için her bir anten 50 Ohm bağlaşımlı düzlemsel dalga (BDD) kılavuzu besleme ucu ile uyarılmıştır. Antenler birbirlerinden bağımsız olarak değerlendirilmiş ve bir ağ inceleyici kullanılarak S11 ve S12, VSWR, verim, kazanç ve bant genişliği değişkenlerine göre incelenmiştir. Sonuç olarak kıvrımlı anten tasarımlarının iyi bir tasarım olduğu ortaya konulmuştur.

ACKNOWLEDGEMENTS

I would like to express my gratitude to my advisor Prof. Dr. Ali Serpengüzel for the continuous support of my M.S studies and related research. His guidance helped me in all the time of research and writing of this thesis.

Besides my advisor, I would like to thank my thesis committee members: Prof. Dr. Hilmi Ünlü and Associate Prof. Dr. Kaan Güven for their valuable time, guidance and constructive comments.

I am thankful to Associate Prof. Dr. Kaan Güven, who gave access to the laboratory and research facilities. Without his precious support, it would not be possible to conduct this research.

I would like to express my gratitude to Dr. Ulaş Sabahattin Gökay, and my colleagues at Koç University Microphotonics Research Laboratory for their help and cooperation on all research matters. I am immensely thankful to Mr. Selçuk Çakmak for his help and guidance, whenever required.

I would like to thank Higher Education Commission (HEC), Pakistan for sponsoring my studies, abroad.

This thesis is dedicated to my parents and siblings,
for their endless love, support, and encouragement.

TABLE OF CONTENTS

List of Figures

List of Tables

NOMENCLATURE

β	Propagation vector in waveguide
c	Speed of light in vacuum
Cs	Capacitance of substrate
$E_{\perp}$	Perpendicular electric field
$E_{//}$	Parallel electric field
ε_r	Dielectric constant of the substrate
η	Impedance of the free space
f_H	Highest frequency in the band
f_L	Lowest frequency in the band
f_o	Resonant frequency
Ga	Conductance of coplanar waveguide
h	Depth of the meandering loops
H	Height of substrate
L	Inductance
Ls	Inductance of source
λ	Wavelength of light in vacuum
M	Number of meandering loops
P_i	Incident power
P_r	Radiated power
ϕ	Azimuth angle
RL	Return Loss
Rs	Resistance of source
S	Metal Spacing
θ	Elevation angle
T_{and}	Loss tangent
T_{met}	Conductor thickness
$VSWR$	Voltage standing wave ratio
w	Coupling width

W	Metal width
ω	Radial angular frequency
Z_o	Input impedance

1 INTRODUCTION

The origin of antennas goes back to 1830s' when Michael Faraday demonstrated the coupling between electricity and magnetism, long before Maxwell's equations were formulated. A magnet was slid in proximity of coils. The coils were attached through a wire to a galvanometer. A time-varying magnetic field caused a time-varying electric field. Electromagnetic radiations were detected and the coil behaved as a first loop antenna [1,2].

According to IEEE Standard Definitions of Terms (IEEE Std 145-1983): "An antenna is any device, that converts electronic signals to electromagnetic waves (and vice versa)" [3].

Today an antenna is the heart of any wireless communication system. The antenna works as an efficient transducer between RF signal and free space, with minimum conversion losses. Alternatively, the antenna coverts 50 Ohm input impedance from a device to 377 Ohms free space impedance, or vice versa. Antennas are known for their reciprocity behavior (that is, no behavioral difference in an antenna in receiving or transmitting configuration) [4]. An antenna is a passive device, the antenna does not amplify the signal but the antenna may have a higher gain in one direction and depending on the design [5].

Meandering antennas are growing in popularity, because of their low profile structures. Meandering antenna is a special type of microstrip patch antenna, and is mainly used for the purpose of miniaturization. Instead of a conducting patch with plane geometry and dimensions, a meander is relatively complex, designed in a way to achieve optimal path length within a limited physical space. Meandering antennas are relatively complex to analyze and entail numerical computations. Reduced resonant length is achieved through continuously folded wires. It was found that, size reduction gets better as the wire radius decreases [6]. It has been demonstrated that, for a fixed length of a wire, improved size reduction can be achieved by increasing the width to wire radius ratio [7]. Meandering antennas are well compatible for embedded designs in mobile wireless devices, telemetry, and communication. Less thickness and conformal design makes, this class of antennas, a suitable choice for certain high end applications, like airborne platform, where conformance is a highly desired parameter to ensure required aerofoil profile [8]. Light weight, compact size, conformance to the surface, low fabrication profile, ease of integration to the platform and physically robust are some upsides associated with this class of antenna. Limited bandwidth (BW), compromised efficiency, small gain, spurious radiation from feed probe, and limited power capacity are downside associated to meandering line antennas [9]. Overall, meandering antennas designs present various design challenges, but show a great promise for the wireless applications.

Meandering antennas are narrow BW, wide beam antennas that offers high flexibility in terms of fabrication. Fabrication entails etching the meandering line pattern over a metal coated dielectric substrate, commonly referred as printed circuit board (PCB) [10]. A PCB could be single or double sided with a uniform metal cladding bonded to dielectric substrate. The thickness of the bonded metal is measured in Ounces (Oz), and is typically one or two Oz. Low dielectric constant substrates are generally preferred for high radiation. Relative permittivity and loss tangent determine the choice of the dielectric substrate [11]. Generally one of the layers serves as ground and the other as conductor; however in a single layer design both conductor and ground are on the same plane as shown in Figure 1.1. A meandering antenna is characterized by length of the meander, width, and twist angle.

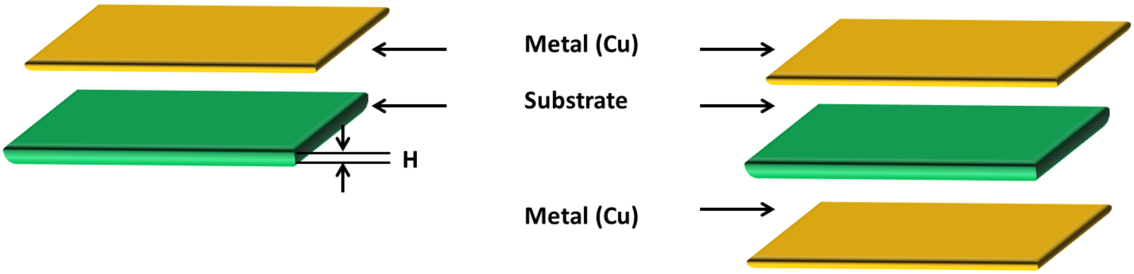

Figure 1.1: Single vs. double sided PCB.

1.1 Wide band Applications

Wide band and technology attracts a lot of attention from the researchers in recent years due to various design advantages. Several applications of wireless communications require broadband and even ultrawide band (UWB) antennas [12]. Broad band antennas are becoming more desirable as a result of growing demand of bandwidth, for example, video conferencing; direct sequence spread spectrum (DSSS) communication system and frequency hopping, where communication security and anonymity is employed at the cost of much higher bandwidth. UWB technology makes use of pulses of width of the order of nano seconds, hence broadening the spectrum and turning the power density below noise level. This technique offers promising advantages like jamming immunity and improved performance against multipath effects [13], and has penetration capability as its spectrum includes low frequency components. Because of these outstanding features, UWB technology has enormous applications in wireless communications, wireless sensor network (WSN), medical, tracking and localization applications [14]. In addition, UWB provide security and low power consumption that increases the battery life of the portable terminals [15].

1.2 Research Methodology

Wideband meandering antennas are presented in this thesis. In order to evaluate the performance for suitable comparison, six designs are implemented using a 50-Ohm

Coplanar Waveguide (CPW) as feeding probe. Antennas are modeled and simulated using finite element method (FEM) and measurements are carried out on a Network Analyzer (NA), which include port reflection, transmission, VSWR, radiation pattern and bandwidth. Antennas with the specifications shown in Table 1.1 are studied and measured in this work.

S.No	**No. of meanders**	**Coupling width (w)**	**Depth (h)**	**Width (s)**	**Wire Thickness (b)**
1.	2	0.075	15.04	15.162	1.05
2.	4	0.075	15.04	22.275	1.05
3.	6	0.075	15.04	29.085	1.05
4.	8	0.075	15.04	35.895	1.05
5.	10	0.075	15.04	43.705	1.05
6.	12	0.075	15.04	51.515	1.05

*all units in mm

Table 1.1: List of antenna design sets.

1.3 Thesis Overview

The theory of antenna performance parameters are explained in chapter 2. These parameters define the figure of merit for a design. A mathematical relationship among the design parameters is investigated in Chapter 3. These parameters founded the base of simulations. Designs are conceived based on the calculated/theoretical expressions and simulations are performed on FEM numerical tool. The simulation results are elaborated in Chapter 4. Design is optimized, in line with fabrication limitations and availability of the material/components. Chapter 5 presents the experimental setup to carry out the characterization measurements. Thesis work is concluded in chapter 6 and recommendations for future work using similar design topologies for different technological applications are submitted.

2 Theoretical Background

2.1 Antenna Parameters

The antenna parameters characterize performance measurement of an antenna. In this part antenna terms like bandwidth (BW), radiation pattern, gain, polarization, and input impedance are explained [16].

2.1.1 Band Width

BW is one of the prime antenna parameters. BW describes the range of frequencies over which, the input impedance, voltage standing wave ratio (VSWR), radiation pattern, and gain are within acceptable ranges from the center frequency. Generally, BW is the basic factor to decide on an antenna [17].

BW is treated as function of reflected power and VSWR. BW is often expressed in terms of percent bandwidth, because the percent bandwidth is constant relative to central frequency (f_c).

$$\%BW = \frac{f_H - f_L}{f_c} \times 100 \quad (2.1),$$

where f_H is the highest frequency, f_L is the lowest frequency and f_C is the center frequency of the band.

2.1.2 Polarization (P)

Electric field vector determines the polarization of an electromagnetic (EM) wave. The polarization is said to be linear, if the electric field vector is always in one plane.

Vertical and horizontal polarizations are two possible cases of linear polarization. Typically electric field vector is taken with reference to the surface of the Earth to classify the polarization as vertical or horizontal [18].

Another type of polarization is called the elliptical polarization, where, the E field vector rotates about a line parallel to the direction of propagation, and E field tip traces out an ellipse. Circular polarization (CP) is a special case of elliptical polarization, in which the electric field vector tips in a circular fashion.

For all practical purposes, the polarization of both the receiving and transmitting antenna must be matched to ensure the maximum power transfer. 3 dB losses occur, if the polarizations are mismatched by 45^o and, reaches 20 dB if mismatch is 90^o [19]. The antenna designed in this work is linearly polarized.

2.1.3 Return Loss (RL)

RL is related to impedance matching and its origin lies in maximum power transfer theory, and gives the measure of effective power transfer from RF source to the antenna. Any mismatch will cause return loss. The return loss (RL) is defined by the ratio of the incident power of the antenna P_t to the power reflected back from the antenna P_r [20]. The mathematical expression for RL is given by:

$$RL = 10\log\left[\frac{P_i}{P_r}\right] = -20\log\left[\frac{E_r}{E_t}\right] = -20\log\left[\frac{VSWR-1}{VSWR+1}\right] \quad (2.2)$$

For optimal power transfer, the return loss should be lower than -10 dB. This parameter is referred as S11 in this thesis.

2.1.4 Radiation Pattern (θ, φ)

As per the standard IEEE definition, radiation pattern is “the spatial distribution of a quantity that characterizes the electromagnetic field generated by antenna” [21]. Radiation pattern is represented in two or three dimensional spatial distribution. Radiation pattern is a function of the observer’s position along a path or surface of constant radius [22] and goes through a direction at which maximum radiation occurs. Spherical coordinate system is used to visualize the radiation pattern. A two dimensional pattern can be a function of the elevation angle θ, at constant azimuth angle φ, or a function of φ at constant θ value [23].

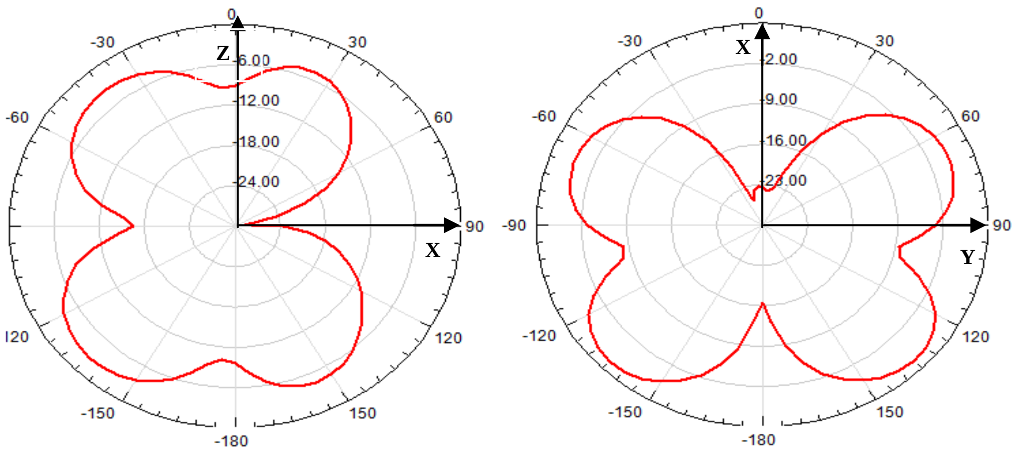

Figure 2.1:A typical radiation pattern (a) elevation plane *f* (θ) (b) azimuth plane *f* (φ).

2.1.5 Directivity D (θ, φ)

As per standard IEEE definition directivity is defined as “the ratio of the radiation intensity in a given direction from the antenna to the radiation intensity averaged over all directions” [24]. It is often defined only to the direction of the major lobes. Directivity function $D(\theta,\phi)$ describes the variation of the radiation intensity. The directivity function $D(\theta,\phi)$ is defined by:

$$D(\theta,\phi)=\frac{\text{Power radiated per unit solid angle}}{\text{Average power radiated per unit solid angle}} \qquad (2.3).$$

If P_r is the radiated power, the $\frac{dP_r}{d\Omega}$ gives the amount of power radiated per unit solid angle. Had this power been uniformly radiated in all directions, the average power radiated per unit solid angle would be $\frac{P_r}{4\pi}$.

2.1.6 Gain

The antenna gain G (θ, φ), is similar expression as the directivity, except it takes into account the total input power delivered to the antenna port, which is P_{in}, used as the reference rather than the total radiated power. The amount of power given as input to the antenna is not fully radiated, and is mathematically related by the radiation efficiency of the antenna:

$$P_r = \eta P_{in} \qquad (2.4),$$

where η is the radiation efficiency of the antenna, and the gain of the antenna is defined as:

$$G(\theta,\phi) = 4\pi \frac{\text{radiated power per unit solid angle}}{\text{input power}} \qquad (2.5).$$

The gain can also be defined with a relation to the radiation efficiency and the directivity function as;

$$G(\theta,\phi) = \eta D(\theta,\phi) \qquad (2.6).$$

The maximum of the gain function is termed as the gain of the antenna.

2.1.7 Axial Ratio (AR)

The AR is the measure of the polarization of an antenna. It is defined as the ratio of the major axis to the minor axis of the polarization ellipse [25]. The ellipse can be characterized by its maximum and minimum field values, $|E_{max}|$ and $|E_{min}|$, respectively. The axial ratio (AR) of the ellipse is defined by:

$$AR=\frac{|E_{max}|}{|E_{min}|} \quad (2.7)$$

For practical purposes the axial ratio (AR) is represented in dB and ‘0’ amplitude defines circular polarization, moderate values (up to few dBs) refer to elliptical polarization and higher values refer to for linear polarization. In this thesis, the polarization value is measured in tens of dBs and qualifies the definition of linearly polarized antenna.

3 Antenna Modeling

3.1 Principle of Operation

The basic operating principal of a meandering antenna is based on current distribution. A conductor traces line on a flat dielectric substrate surface. The centre conductor lines serves as the feed line to couple electromagnetic (EM) energy in or out of the radiating patch. The current in the adjacent arms flows in the opposite directions. The radiation effects of the vertical current are cancelled out in a symmetric geometry, and only horizontal component effects the radiation in far field of an antenna. This in return affects radiation resistance and eventually the gain and efficiency are limited for this class of antennas [26]. The current in the adjacent arms creates electric field which extends to the outer periphery. These field extensions, known as fringing fields cause the conductor to radiate.

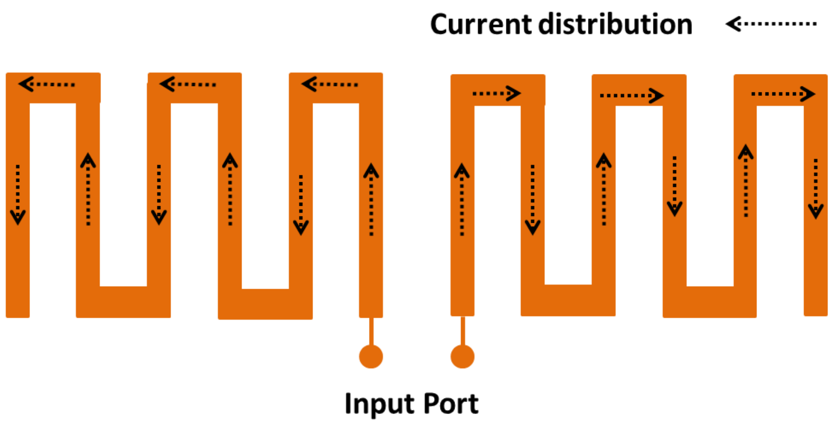

Figure 3.1: Principal of operation of meandering antenna.

Many designs techniques are improvised in recent years to achieve broad bandwidth (BW) antennas. This can be achieved by using different feeding shapes and configurations such as coplanar waveguide (CPW) and unconventional ground plane approach. [27].

In this work, broadening of the BW is achieved by using a CPW feeding probe and complementing together the closely spaced resonance response of multiple meanders. Multiple meanders introduce longer current paths and hence add multiple/broad staggered resonating modes. This design technique is used to achieve multiband designs using resonating modes far from each other. However, if the design is modified to let these resonances come closer to each other, they will complement the effect of closely spaced resonances forming staggered resonating behavior and broadband antenna structure is achieved [28]. It is known that, the substrate height (H) is proportional to the BW and as height (H) is extended to infinity by eliminating the ground plane the BW becomes very wide [29]. Thick substrate excites higher order modes which enables broad bandwidth scenario. A further exaggerated scenario of multiple higher order modes, in close proximity will lead to ultra-wideband response. Another explanation for the conductor lines printed on dielectric substrate is cylindrical monopole antenna flatted to be plane (radius extended to infinity) and it is known that bandwidth is proportional to the diameter of the metallic rod [30] and higher modes are excited as a function of infinite radius. Upon optimizing the dimensions of the antenna, these higher order modes could be close to each other to yield very broad bandwidth response.

In designing methodology, the lower frequency (f_L) response is first established and then bandwidth is extended to higher frequency (f_H) end. Path length ‘s’, thickness ‘b’, depth ‘h’, number of meanders ‘M’ and substrate thickness affects both F_L as well as the bandwidth (BW) , and optimization is needed to achieve required bandwidth (BW) as well as the lower frequency (f_L). Another important design parameter that affects the bandwidth (BW) is the feed probe itself. As long as there is no abrupt transition in the dimensions of the feed lines to the radiator, we obtain broader bandwidth (BW) [31]. Using CPW instead of conventional feed enhances the bandwidth (BW) response of an antenna [32].

3.2 Coplanar waveguide feed (CPW)

CPW offers strong merits over conventional feed probe, such as low radiation losses, dispersion, easy realization of design parameters with reference to the input impedance and relative permittivity, and uniplanar configuration transmission. CPW is one of the preferred choices in embedded systems and active solid-state devices [33]. To classify a feed probe as CPW, following conditions need to be satisfied:

(a) A conductor separated from the pair of grounds,
(b) All conductors on the same plane,
(c) All conductors atop a dielectric medium.

CPW is employed in this design and geometry parameters are calculated using an online software [34,35]. Figure 4 shows the design parameters and calculations performed. A summary of input parameter is shown in Table 3.1.

Parameter	**Symbol**	**Value(s)**
PCB dielectric constant	ε_r	4.4
Conductor thickness	T_{met}	0.035 mm
Operating frequency	f_o	10 GHz
Substrate height	H	1.6 mm
Metal width	W	4 mm
Metal Spacing	S	0.5 mm
Loss tangent	T_{and}	0.02

Table 3.1: Input parameters for CPW.

Figure 3.2 represents the generic description of a CPW and the parameters that formulate the mathematical relationship among the input and output parameters as show in Table 3.1 and Table 3.2 respectively. The equivalent circuit for CPW is shown in figure 3.3.

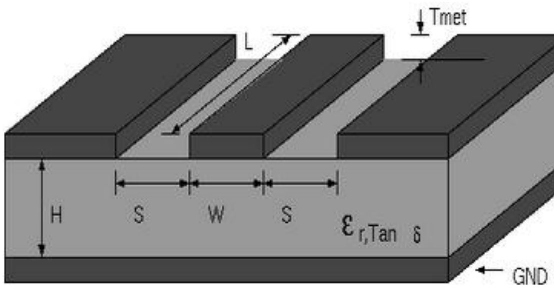

Figure 3.2: CPW geometry and equation parameters.

Parameter	Symbol	Value(s)
Inductance	***Ls***	0.2593 nH/mm
Resistance	Rs	21.63 mOhm/mm
Capacitance	*Cs*	0.1017 pF/mm
Conductance	*Ga*	177.52 uMhs/mm
Input impedance	*Zo*	50 Ohm
Skin depth	σ	0.000660 mm

Table 3.2: Output parameters for CPW.

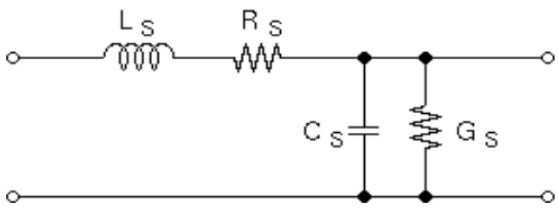

Figure 3.3: CPW equivalent circuit.

3.3 Resonant Frequency Calculation for the meandering antenna

The geometry is realized as inserting meanders on a dipole. The meanders increase the inductive reactance of the antenna. The resonant frequency of the dipole significantly changes in response to the additional meanders. However, if the length of the dipole with meanders is shortened to decrease the inductive reactance, it is assumed that shortened meanders capacitive reactance remains the same as that of the standard dipole, it still resonates at the frequency, which the dipole does.

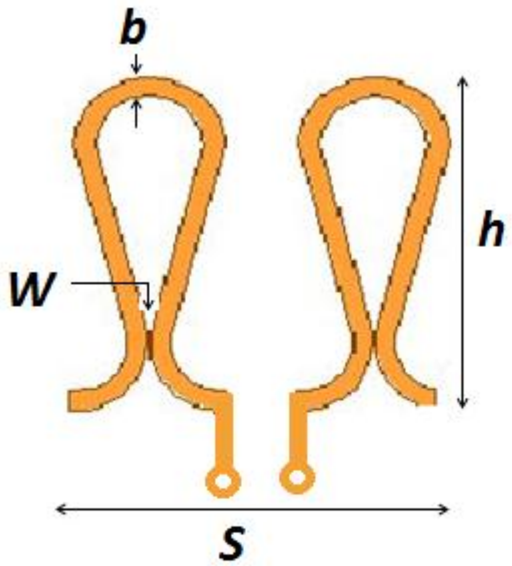

Figure 3.4: Meander geometry that corresponds to a dipole of length‘s’.

As a result, meander’s resonant frequency is the same as that of a dipole and the inductive reactance should be approximately the same. Figure 3.4 shows the physical parameters used in the calculation of the resonant frequency. The derivation of resonant frequency as a function of physical parameter goes as follow:

$$Z_o = \frac{\eta}{\pi}\log\frac{2w}{b} \qquad (3.1),$$

where **w** is the gap width, **b** is the wire width, η is impedance of the free space (377 Ohms) as shown in Figure 3.4.

The input impedance of the transmission line (Z_{in}) is given by the impedance Z_o and the load impedance (Z_L) together with the wave vector (β) and the path length (h) as;

$$Z_{in} = Z_o\left[\frac{Z_L + jZ_o \tan\beta h}{Z_o + jZ_L \tan\beta h}\right] \qquad (3.2)$$

For short termination load impedance $Z_L = 0$ and Eqn. 3.2 modifies as:

$$Z_{in} = jZ_o \tan \beta h \quad (3.3).$$

where

$$Z_{in} = j\omega L \quad (3.4),$$

ω is the radial resonant frequency and L is the inductance

3.4 Inductive Modeling

From Eqn. 3.1, 3.3 and 3.4, we calculate the inductance of an individual loop as;

$$L = \frac{\eta}{\omega\pi} \log \frac{2w}{b} \tan \beta h \quad (3.5).$$

For *M* number of meander lines $L_m = M \times L$.

The straight conducting line, with length's' also results in a self-inductance. It is given by the following equation:

$$L_s = \frac{\mu_o}{2\pi}\left[\log \frac{4s}{b} - 1\right] \quad (3.6).$$

And total inductance L_t is sum of L_m and $L_{s;}$

$$L_t = \frac{\mu_o}{2\pi}\left[\log \frac{4s}{b} - 1\right] + M \frac{\eta}{\omega\pi} \log \frac{2w}{b} \tan \beta h \quad (3.7).$$

The self-inductance of a dipole antenna in relation to resonating wavelength is given by

$$L_d = \frac{\mu_o}{4\pi}\lambda\left[\log \frac{2\lambda}{b} - 1\right] \quad (3.8).$$

Only under resonating condition the inductance of both the dipole and the meandering antenna are the same so that:

$$L_d = L_t \quad (3.9).$$

And the final equation is given by:

$$\frac{\mu_o}{4}\lambda\left[\log \frac{2\lambda}{b} - 1\right] = \frac{\mu_o}{2}\left[\log \frac{4s}{b} - 1\right] + M \frac{\eta\lambda}{2\pi c} \log \frac{2w}{b} \tan \beta h \quad (3.10).$$

The above transcendental equation 3.10 relates the physical dimensions of the meandering antenna as a function of resonance wavelengths. The transcendental equation is numerically solved and the results are summarized in Table 3.3.

Serial No	Meanders	Mode Number	Wire Thickness	Coupling Width	Depth	Length	Calculated Resonance Frequencies	Calculated Resonance Frequencies
-	M	N	b	w	h	s	f_o	f_o
-	-	-	Mm	mm	mm	mm	0- 5 GHz	5- 15 GHz
1.	2	6	1.05	0.075	15.04	15.162	2.37	6.16, 7.13, 9.93, 11.4, 11.84
2.	4	7	1.05	0.075	15.04	22.275	2.4	6.11, 7.1, 9.47, 9.93, 11.26, 11.85
3.	6	6	1.05	0.075	15.04	29.085	2.38	6.09, 9.22, 9.8, 11.25, 11.84.
4.	8	7	1.05	0.075	15.04	35.895	2.41	6.21, 7.1, 8.7, 9.72, 10.67, 11.26
5.	10	7	1.05	0.075	15.04	43.705	2.37	6.21, 7.13, 8.3, 10, 11.35, 11.8,
6.	12	8	1.05	0.075	15.04	51.515	2.38	6.13, 7.13, 8.93, 9.4, 9.72, 11.35, 11.8

Table 3.3: Calculations of resonant frequencies.

3.5 Summary

We discussed theoretical and mathematical realization of the DMW as a resonant antenna. The resonant frequencies are calculated and observed mainly centered around

10 GHz, which is the design frequency for this work. The impedance of CPW depends on resonant wavelength and the dimensions of CPW are calculated for 10 GHz. Any deviation far from 10 GHz would render the 50 Ohms input port matching invalid.

4 NUMERICAL SIMULATIONS

The numerical simulations were performed using finite element method (FEM). The simulation results for all designs are presented in this chapter. The results include S11 parameters, VSWR, radiation pattern, antenna gain, and radiation efficiency.

To ensure the maximum power delivered to the radiating part of the antenna, reflections are aimed be kept at minimum. In this work, the network matching is achieved using coplanar CPW. The design is carefully parametrized to achieve 50 Ohms impedance at the input port. The simulations are performed for different number of meandering loops. The numbers of meanders are even numbers, since we use a symmetric geometry. A 50 Ohms lumped port is used to simulate the excitation of the antenna. The frequency sweep is performed for 10 GHz range with a center frequency of 10 GHz and a step size of 0.05 GHz.

4.1 Antenna Simulated Designs

The physical parameters of the antenna are optimized after many iterations and optimal values of bandwidth (BW), efficiency, and radiation pattern are obtained for dimensions of 62 mm*40 mm*1.6 mm. The substrate is FR4 with a dielectric constant of 4.4 and a loss tangent of 0.02, for all cases. The simulation results are discussed one by one for all the designs.

4.1.1 Two meandering loops antenna

The first design with 62 mm*40 mm*1.6 mm physical dimensions and 2 meanders loop geometry is shown in Figure 4.1.

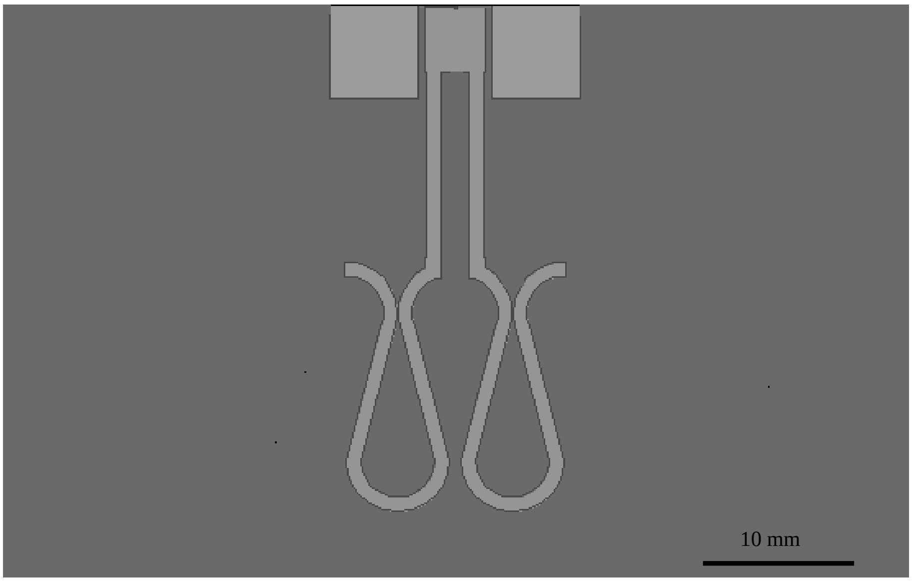

Figure 4.1: Geometry for two meandering loop antenna.

S11 parameters are shown in Figure 4.2. Less than -10 dB return loss is observed for the range from 8.95 GHz to 12.55 GHz (3 GHz BW). The lowest value of return loss corresponds to 11.85 GHz.

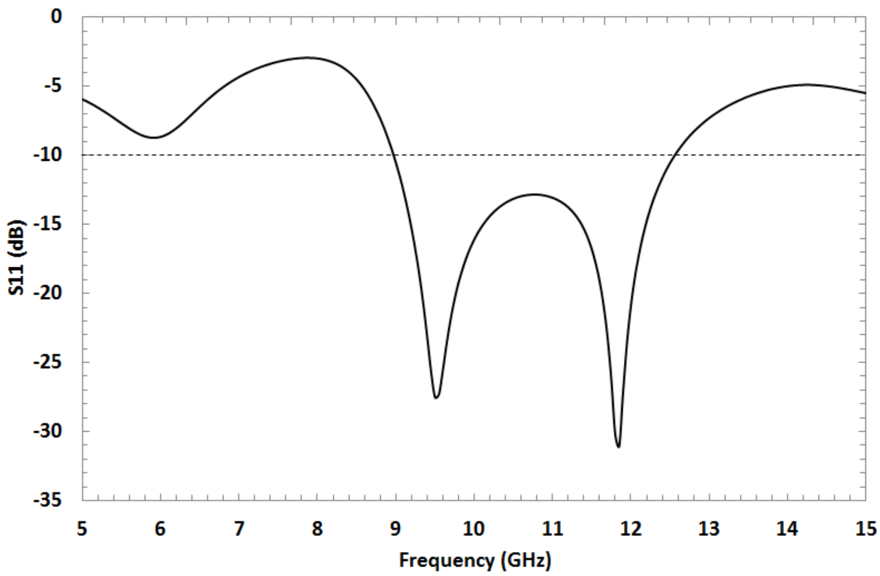

Figure 4.2: Return loss for two meandering loops antenna.

Voltage standing wave ratio (VSWR) is < 2 for the bandwidth from 8.95 GHz to 12.65 GHz as shown in Figure 4.3.

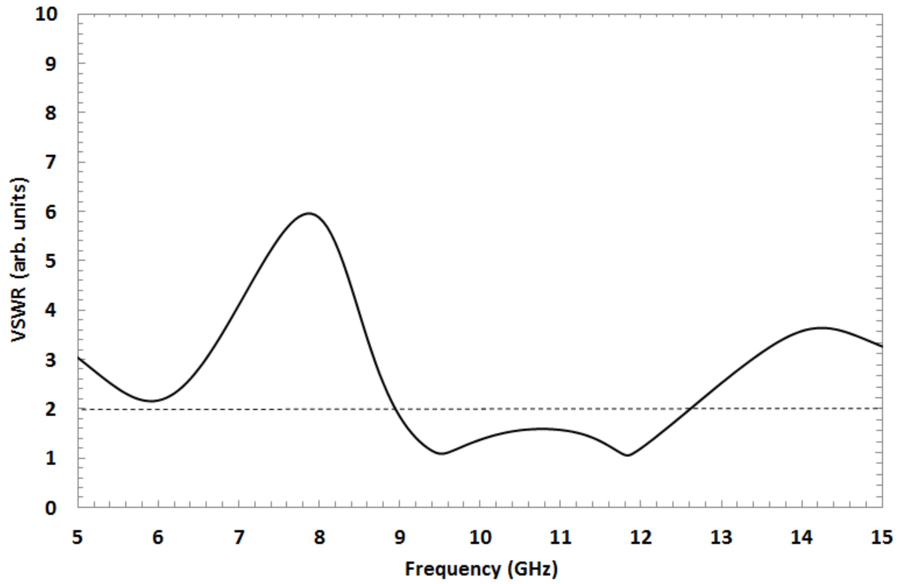

Figure 4.3: Simulation results for VSWR

The radiation pattern for elevation and azimuth plane is recorded and shown in Figure 4.4. The radiation pattern is nearly omnidirectional with nulls observed at the feeding points.

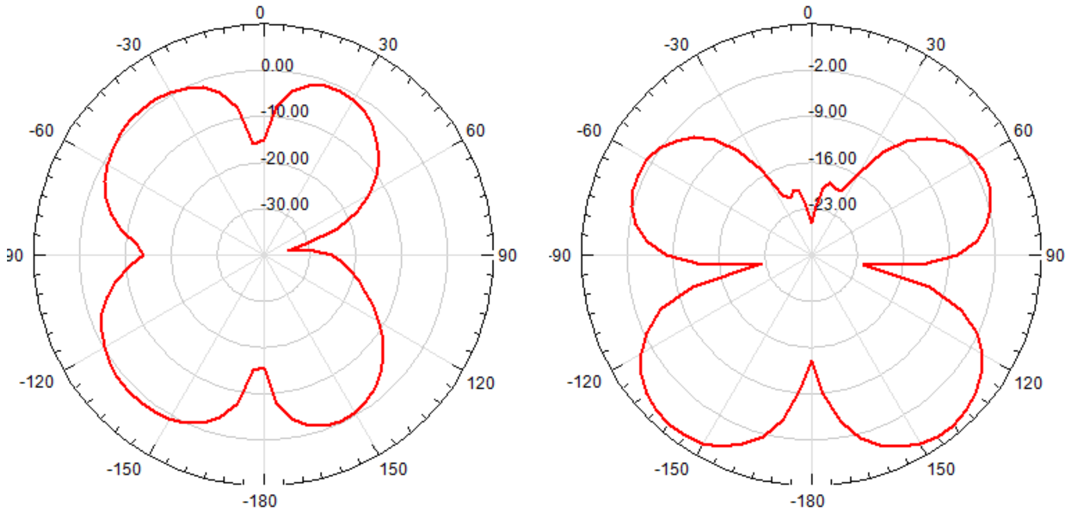

Figure 4.4: 2D radiation pattern with (a) elevation and (b) azimuth plane.

4.1.2 Four meandering loops antenna

The second design with 62 mm*40 mm*1.6 mm of physical dimensions and 4 meandering loops geometry is shown in Figure 4.5.

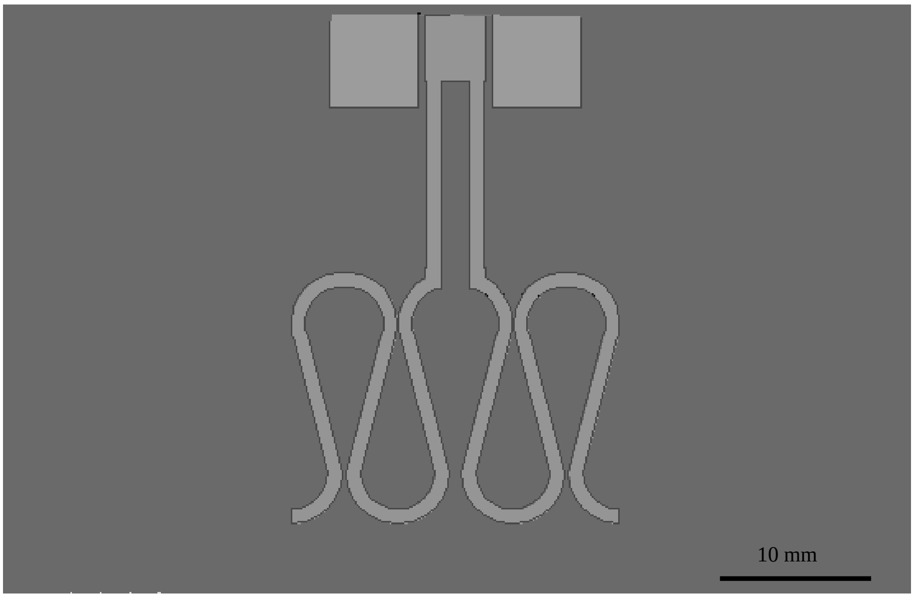

Figure 4.5: Geometry of four meandering loops antenna.

S11 parameters are shown in Figure 4.6. Less than -10 dB return loss is observed for the range from 8.45 GHz to 12.5 GHz (4.05 GHz BW). The lowest value of return loss corresponds to 11.4 GHz.

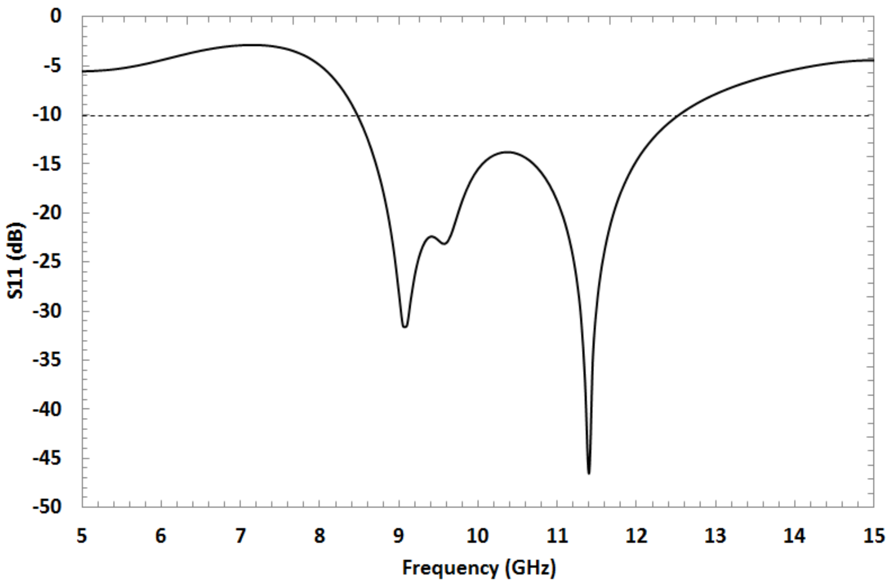

Figure 4.6: Return loss for four meandering loop antenna.

Voltage standing wave ratio (VSWR) is < 2 for the bandwidth from 8.45 GHz to 12.6 GHz as shown in Figure 4.7.

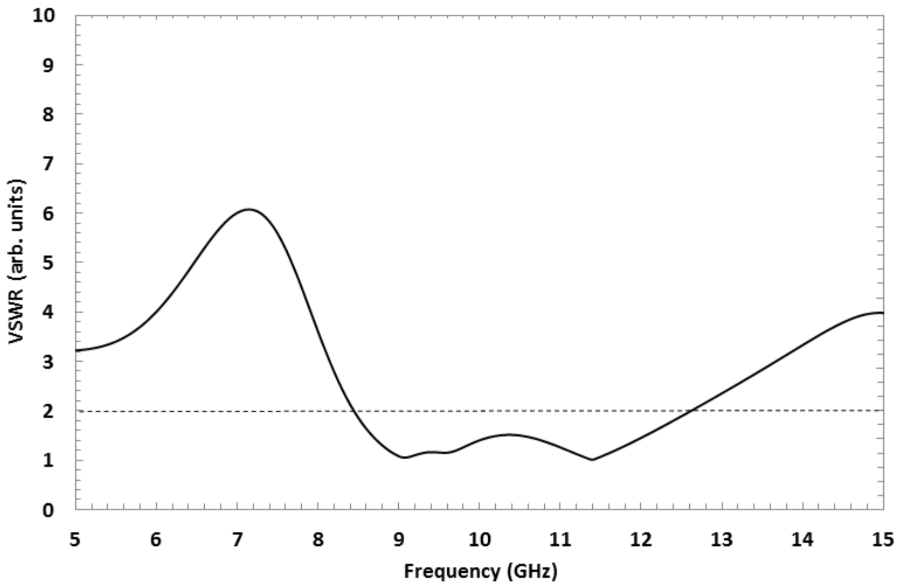

Figure 4.7: Simulation results for VSWR.

The radiation pattern for elevation and azimuth field is recorded and shown in Figure 4.8. The nulls are observed at the feeding points and both patterns are symmetric around the axis of rotation.

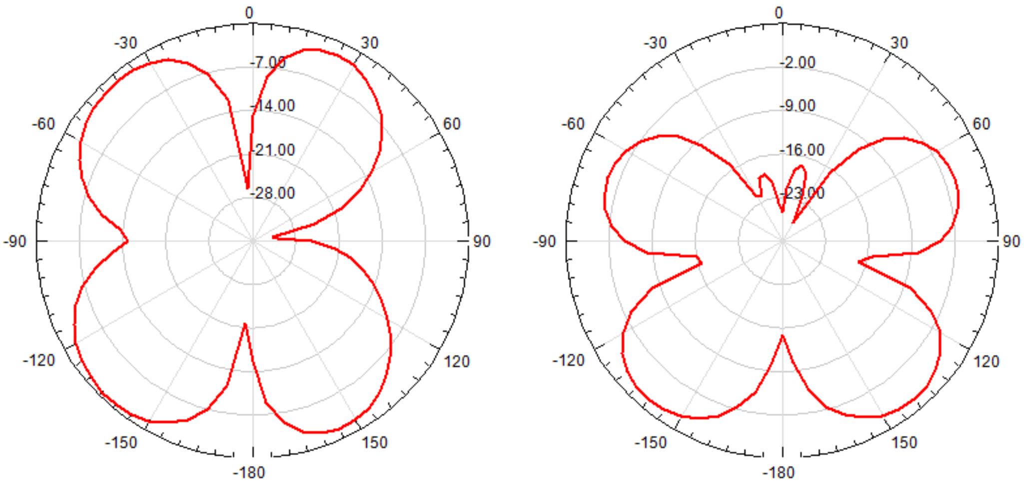

Figure 4.8: 2D radiation pattern with (a) elevation plane and (b) azimuth plane.

4.1.3 Six meandering loops antenna

The third design with 62 mm*40 mm*1.6 mm physical dimensions and 6 meandering loops geometry is shown in Figure 4.9.

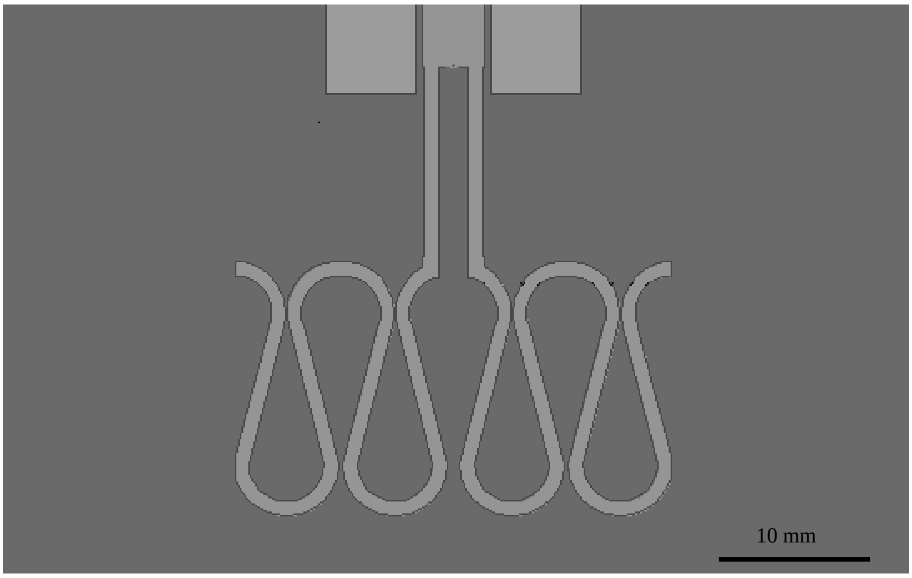

Figure 4.9: Geometry for six meandering loop antenna.

S11 parameters are show in Figure 4.10. Less than -10 dB return loss is observed for the range from 8.2 GHz to 12.6 GHz (4.4 GHz BW). The lowest value of return loss corresponds to 11 GHz.

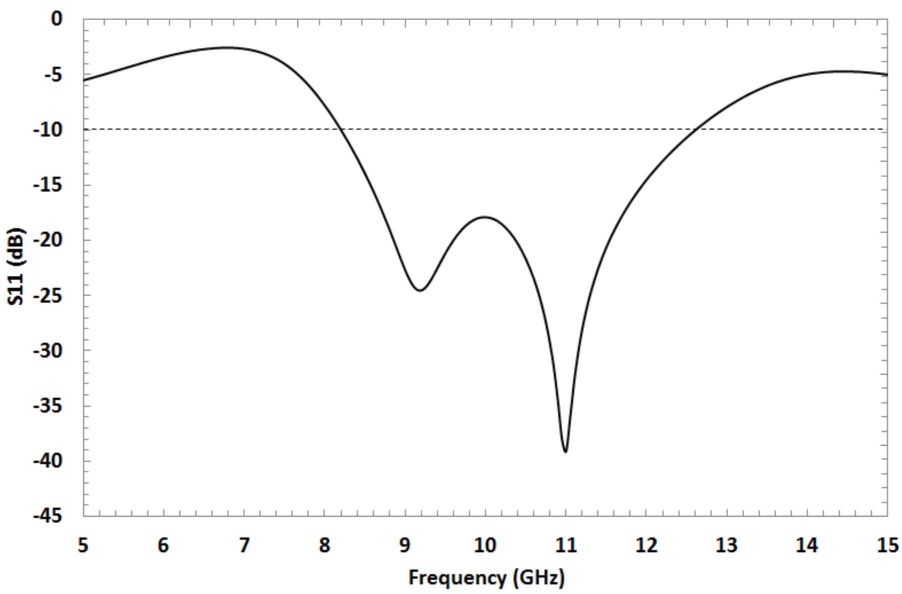

Figure 4.10: Return loss for six meandering loops antenna.

Voltage standing wave ratio (VSWR) is < 2 for the bandwidth from 8.2 GHz to 12.7 GHz as shown in Figure 4.13.

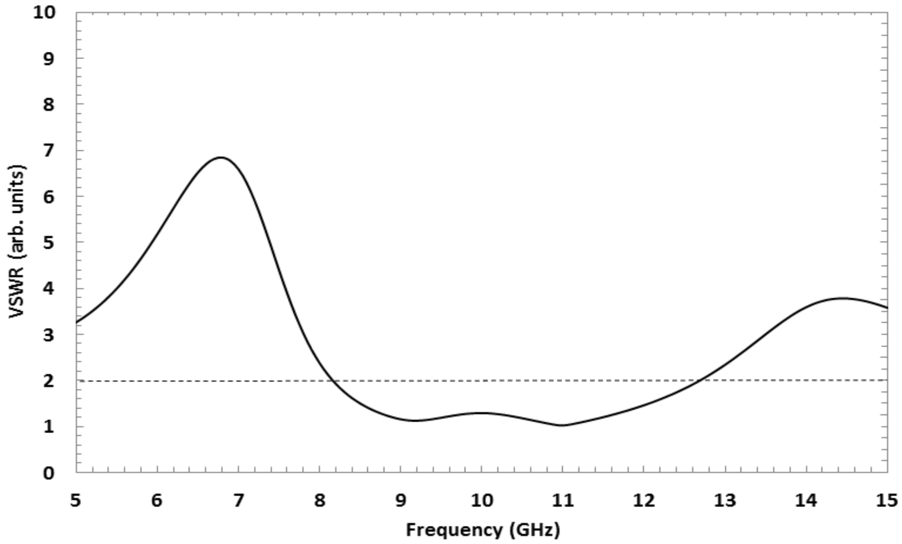

Figure 4.11: Simulation results for VSWR.

The radiation pattern for elevation and azimuth plane is recorded and shown in Figure 4.12. The nulls are observed at the feeding points. The radiation pattern is symmetric around the axis of rotation.

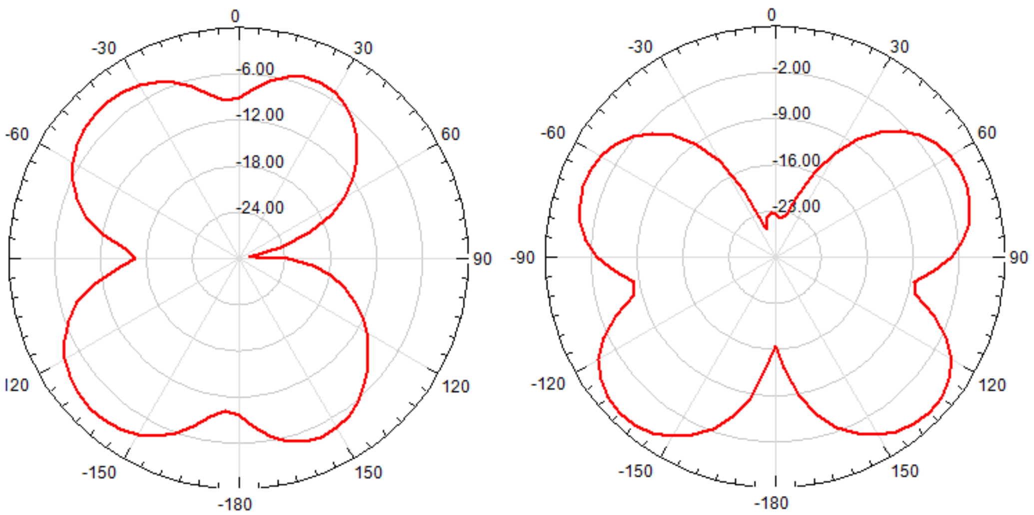

Figure 4.12: 2D radiation pattern for (a) elevation plane and (b) azimuth plane.

4.1.4 Eight meandering loops antenna

The fourth design with 62 mm*40 mm*1.6 mm physical dimensions and 8 meanders loop geometry is shown in Figure 4.13.

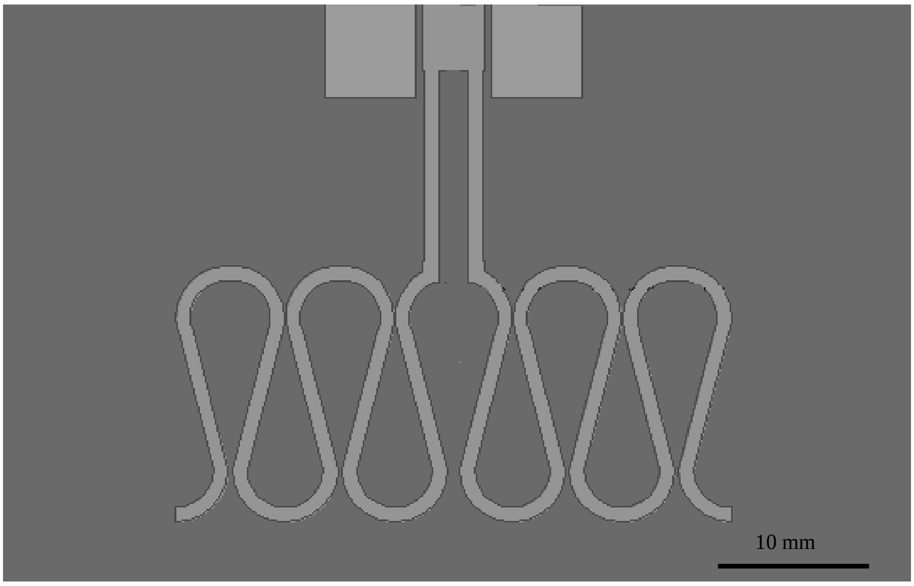

Figure 4.13: Geometry for eight meandering loop antenna

S11 parameters are show in Figure 4.14. Less than -10 dB return loss is observed for the range from 7.85 GHz to 12.35 GHz (4.5 GHz BW). The lowest value of return loss corresponds to 11.55 GHz.

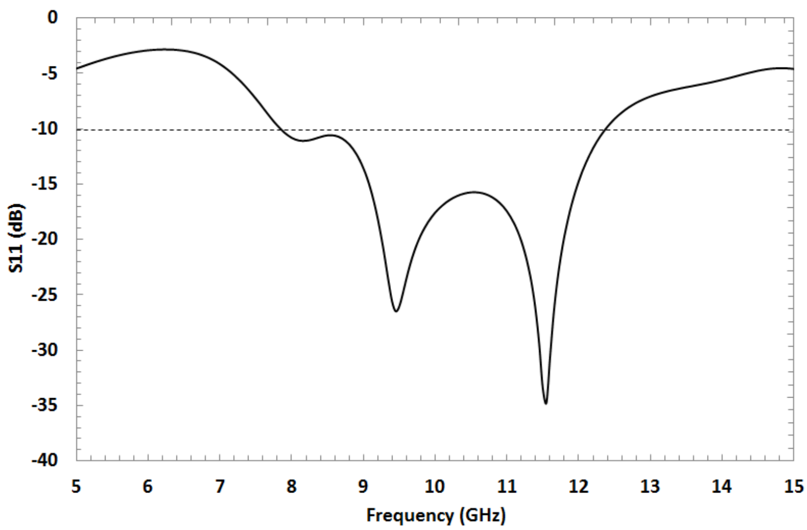

Figure 4.14: Return loss for eight meandering loop antenna.

Voltage standing wave ratio (VSWR) is < 2 for the bandwidth from 7.8 GHz to 12.45 GHz as shown in Figure 4.15.

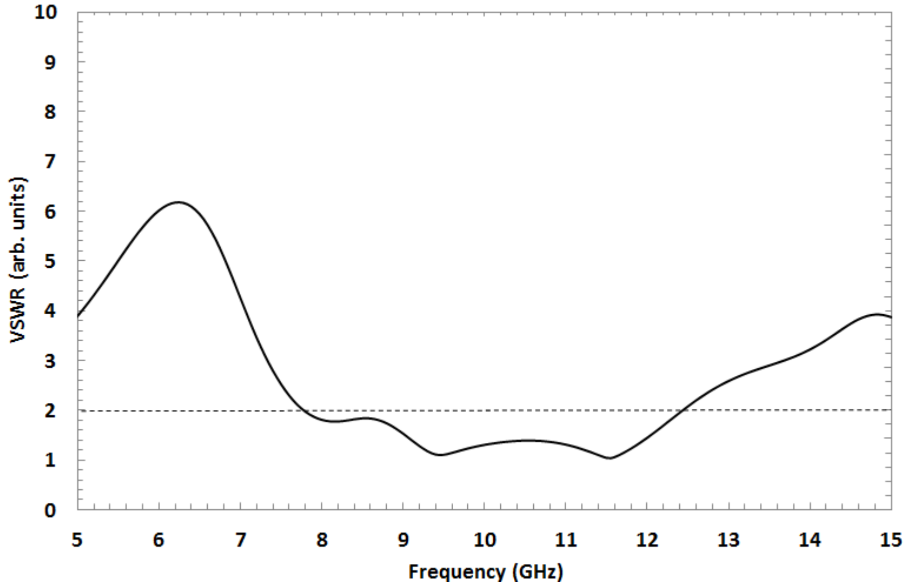

Figure 4.15: Simulation results for VSWR.

The radiation pattern for azimuth and elevation plan is recorded and shown in Figure 4.16. The nulls are observed at the feeding points.

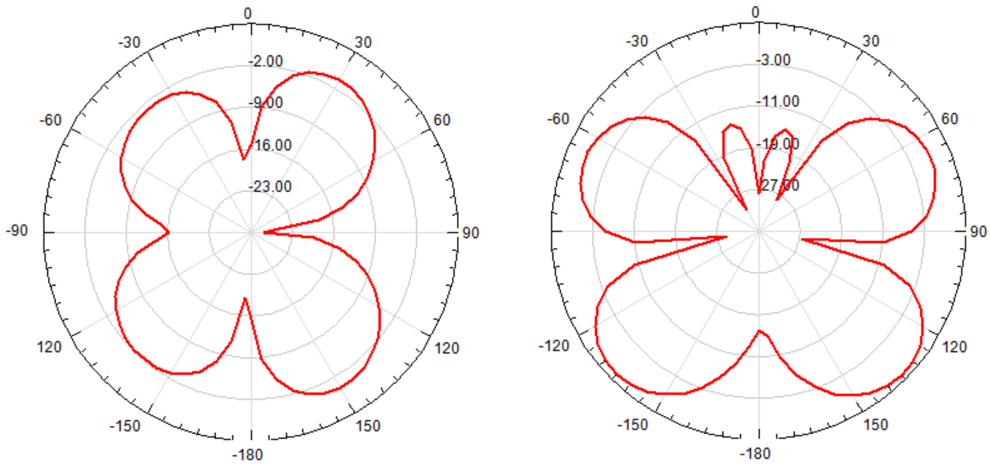

Figure 4.16: 2D radiation pattern with (a) elevation and (b) azimuth plane.

4.1.5 Ten meandering loops antenna

The fifth design with 62 mm*40 mm*1.6 mm physical dimensions and 10 meanders loop geometry is shown in Figure 4.17.

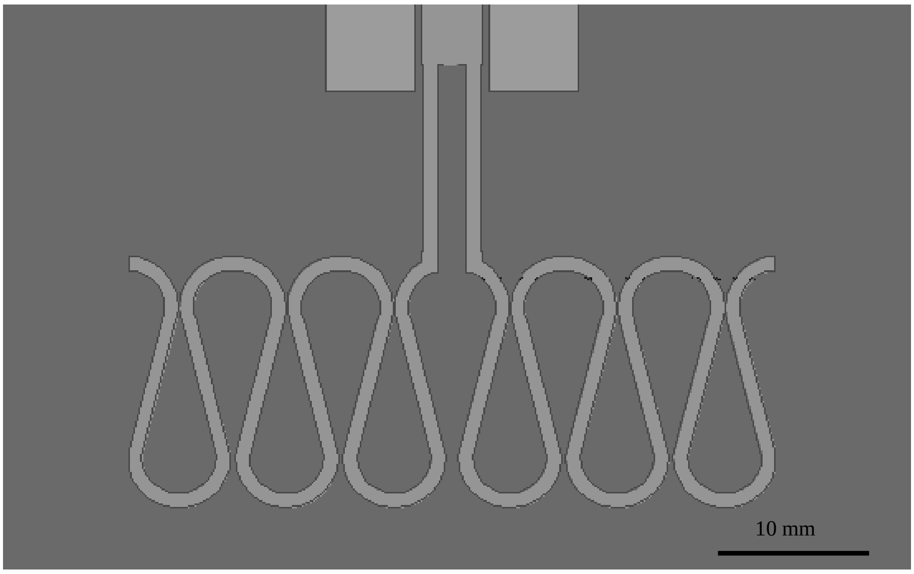

Figure 4.17: Geometry for ten meandering loop antenna.

S11 parameters are show in Figure 4.23. Less than -10 dB return loss is observed for the range from 8.25 GHz to 12.55 GHz (4.2 GHz BW). The lowest value of return loss corresponds to 11.35 GHz.

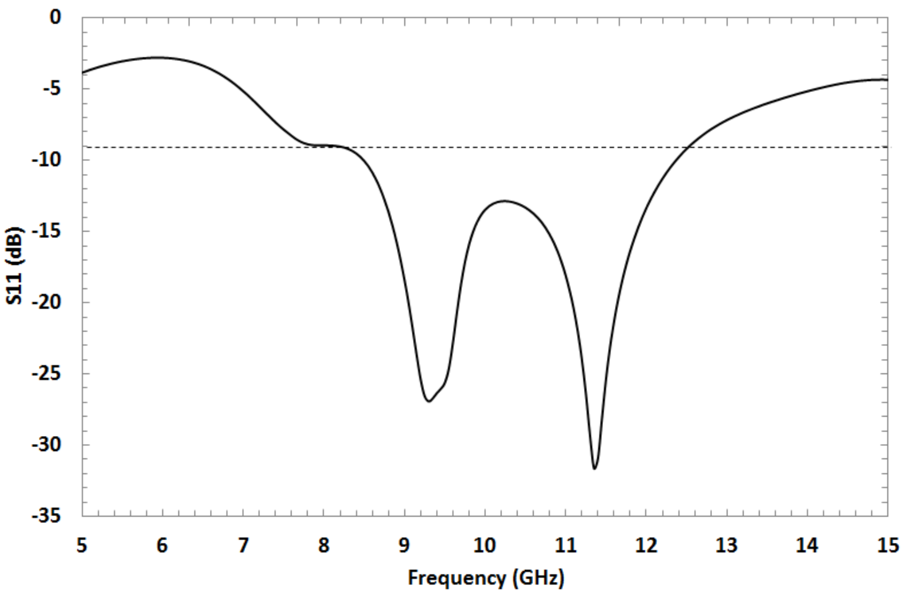

Figure 4.18: Return loss for ten meandering loop antenna.

Voltage standing wave ratio (VSWR) is < 2 for the bandwidth from 8.4 GHz to 12.45 GHz as shown in Figure 4.19.

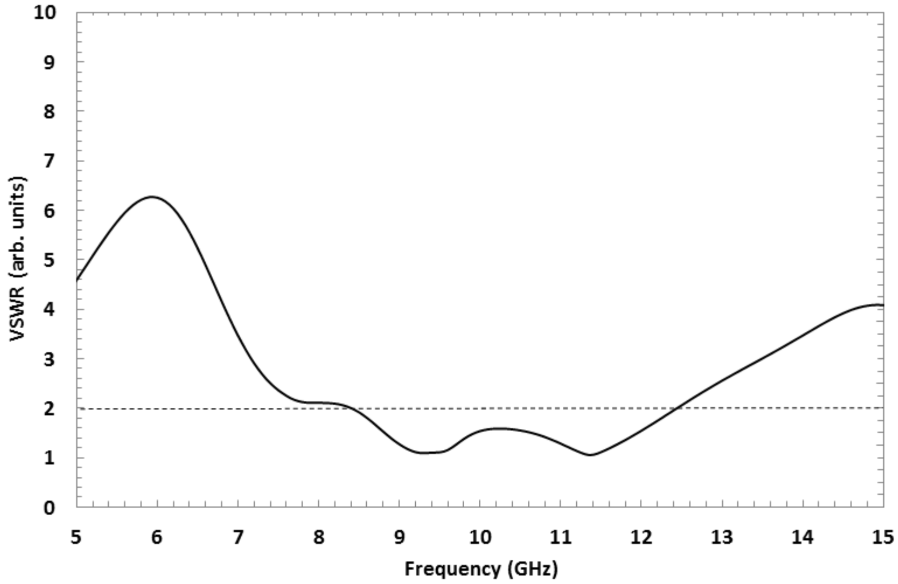

Figure 4.19: Simulation results for VSWR.

The radiation pattern for azimuth and elevation plan is recorded and shown in Figure 4.20. The nulls are observed at the feeding points.

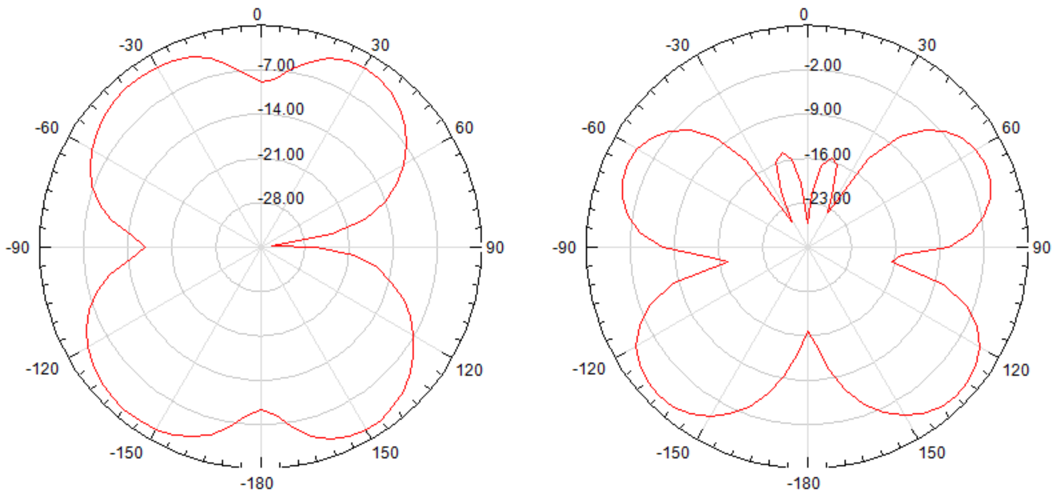

Figure 4.20: 2D radiation pattern with (a) elevation plane and (b) azimuth field.

4.1.6 Twelve meandering loops antenna

The sixth design with 62 mm*40 mm*1.6 mm physical dimensions and 12 meanders loop geometry is shown in Figure 4.21.

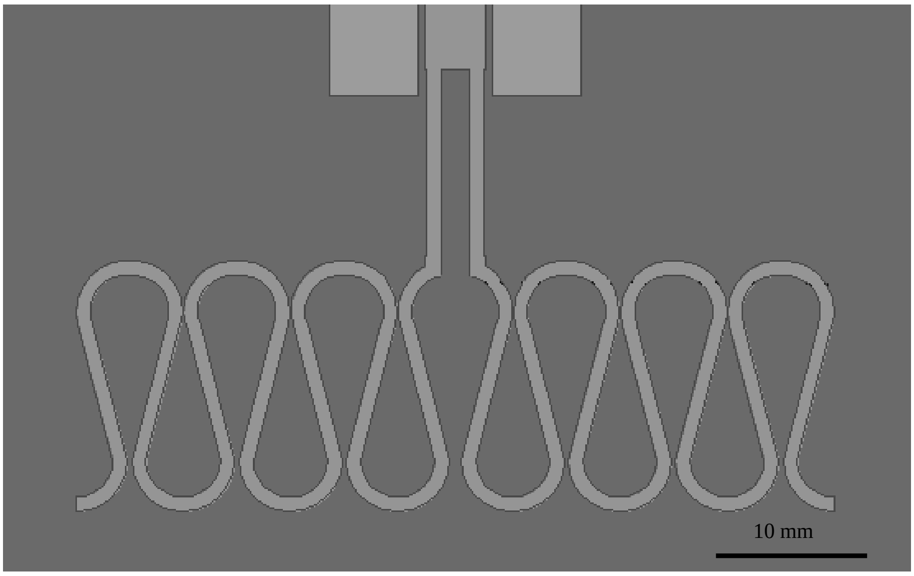

Figure 4.21: Geometry for twelve meandering loop antenna.

S11 parameters are show in Figure 4.22. Less than -10 dB return loss is observed for the range from 8.35 GHz to 12.5 GHz (4.15 GHz BW). The lowest value of return loss corresponds to 9.45 GHz.

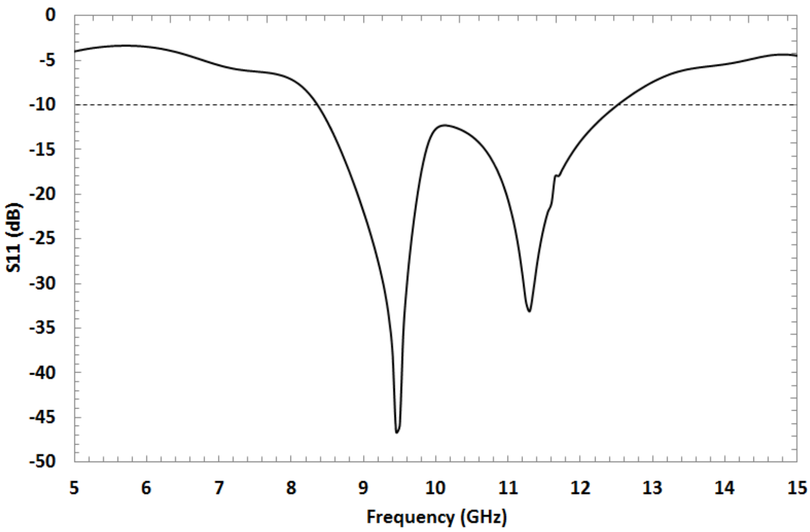

Figure 4.22: Return loss for twelve meandering loop antenna.

Voltage standing wave ratio (VSWR) is < 2 for the bandwidth from 8.3 GHz to 12.6 GHz as shown in Figure 4.23.

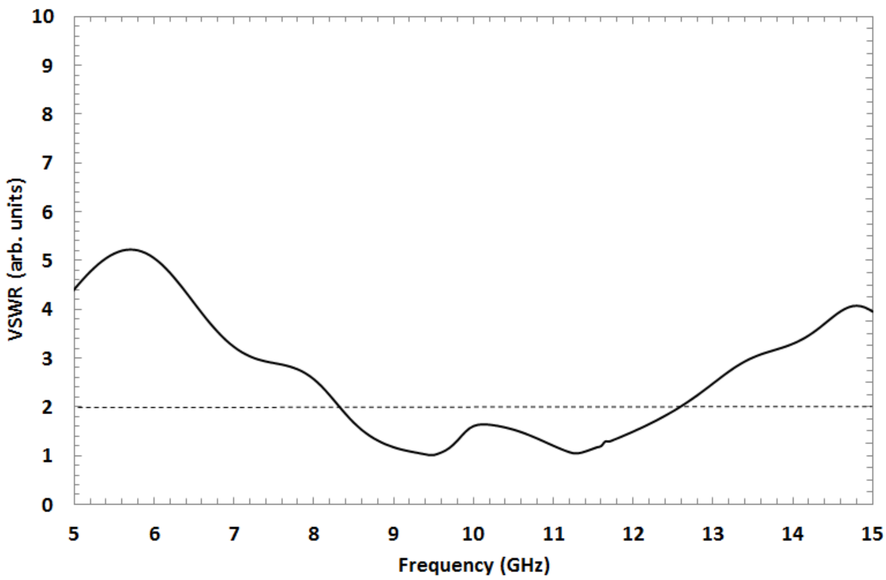

Figure 4.23: Simulation results for VSWR.

The radiation pattern for azimuth and elevation plan is recorded and shown in Figure 4.24. The nulls are observed at the feeding points.

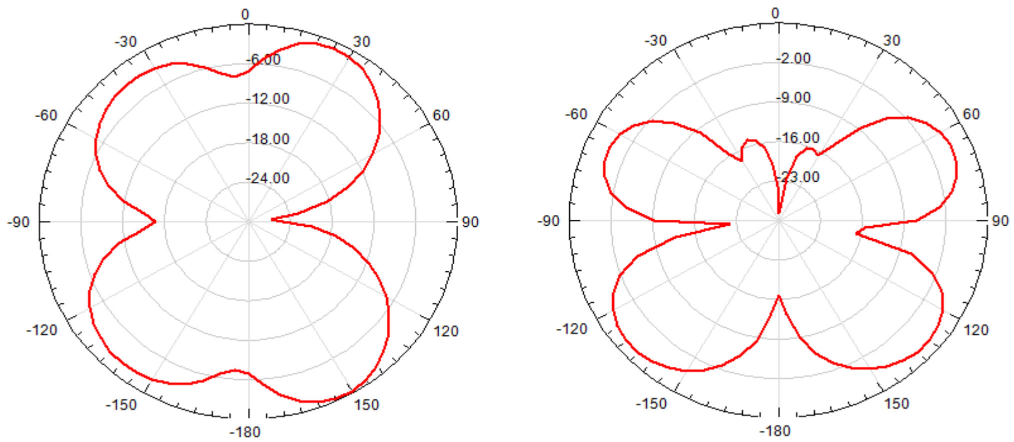

Figure 4.24: 2D radiation pattern with (a) elevation plane and (b) azimuth plane.

The simulation results are summarized in Table 4.1.

Design	**No of meanders**	**Start frequency (f_L)**	**Stop frequency (f_H)**	**BW (Δf)**	**Resonating Frequency (f_o)**	**Gain G**	**Efficiency η**
-	**-**	**GHz**	**GHz**	**GHz**	**GHz**	**dB**	**-**
1	2	8.95	12.55	3	5.85, 9.5, 11.85	2.3	0.88
2	4	8.45	12.5	4.05	9.1, 9.6, 11.4	2.1	0.86
3	6	8.2	12.6	4.4	8.85, 9.45, 11.05	2.2	0.84
4	8	7.85	12.35	4.5	8.15, 9.6, 10.5, 11.5	2.5	0.84
5	10	8.25	12.55	4.2	7.8, 9.3, 11.35	2.1	0.82
6	12	8.35	12.5	4.15	8.9, 9.45, 9.65, 11.3	2.0	0.82

Table 4.1: Meandering loops in relation to efficiency and gain.

4.2 Summary

All designs have promising broad band response and have the ability to radiate in X band. The simulation results are in agreement with the theoretical calculations and resonances are observed around 10 GHz. The efficiency is observed to have inverse proportionality to the number of meanders. The maximum gain is observed for design four with eight number of meandering loops. The highest efficiency is observed for two meandering loop antenna. Eight meandering loop antenna offers the highest BW of 4.5 GHz in contrast to two meandering loops antenna with the lowest value of BW observed to be 3 GHz. 7 % maximum error is calculated between the calculated and the simulated resonant frequencies.

5 RF Measurements

5.1 Antenna Fabrication

The antennas are fabricated using PCB etching technique. The PCB is of the thickness 1.6 mm and substrate material is FR4 epoxy of dielectric constant 4.4 and loss tangent of 0.02. The conductor used in copper of thickness 1 Ounces. The minimum resolution is 75 microns. Twelve meandering loop antennas are fabricated; by cutting away the copper lines. The antenna PCB layout is converted to Gerber format as shown in Figure 5.1.

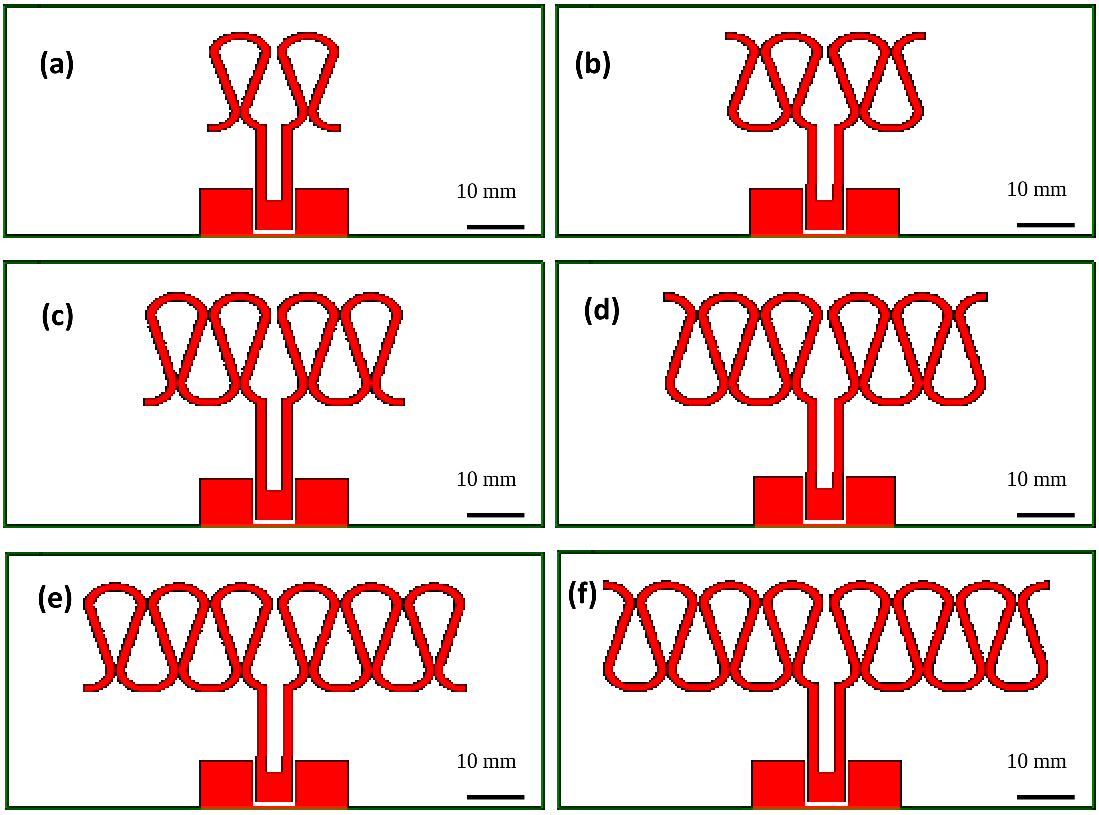

Figure 5.1: Antennas' prototypes in Gerber format.

The antenna is fed with standard 50 Ohms, two holes, female SMA connector. The finished designs are shown in figure 5.2. Each design is similar and only differs by the number of meandering loops.

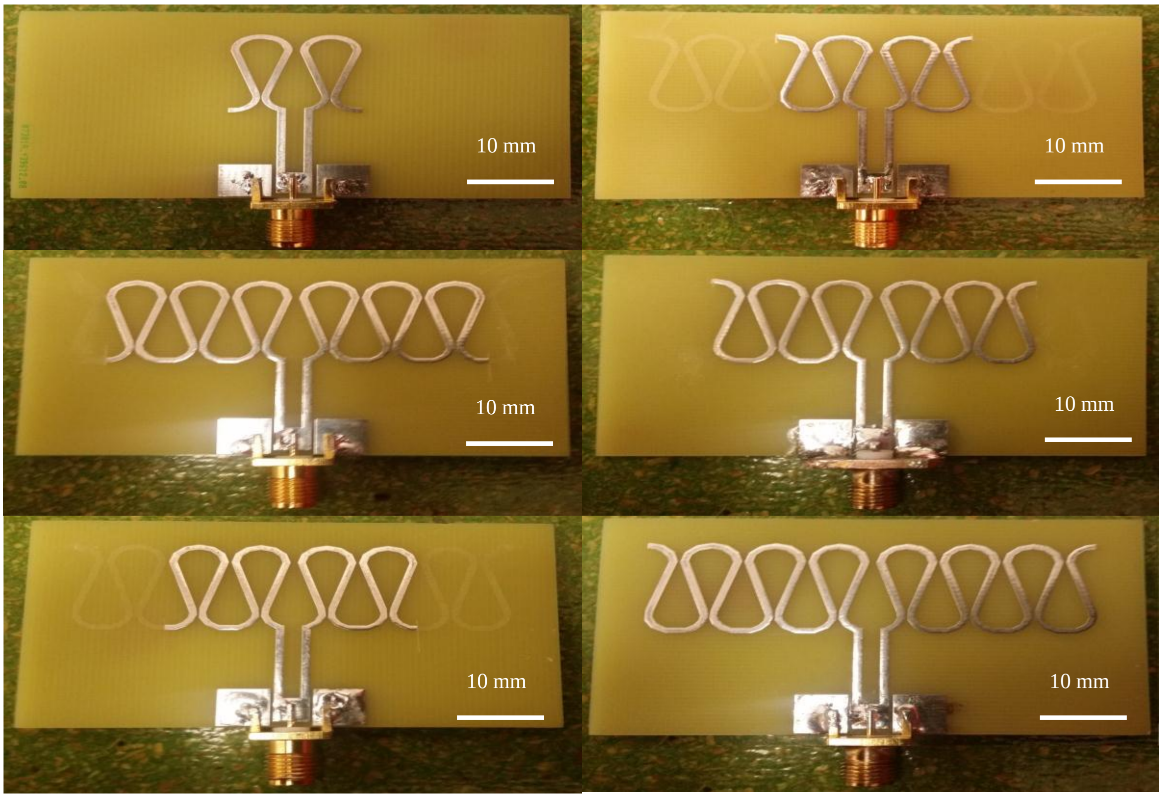

Figure 5.2: Fabricated Antennas with different number of meandering loops.

5.2 Measurements

Agilent 8719ES Network Analyser is used to measure transmission properties of the antennas. Measurement of S11 parameter determines the reflection to the input port of the antennas. All precautionary measures were taken to avoid unwanted reflections from the conduction boundaries, however due to non-availability of anechoic chamber facility, absolute suppression of unwanted reflections have been a challenge. S11, S12 magnitudes, VSWR and radiation patterns for elevation and azimuth angles of the antenna have been measured and presented.

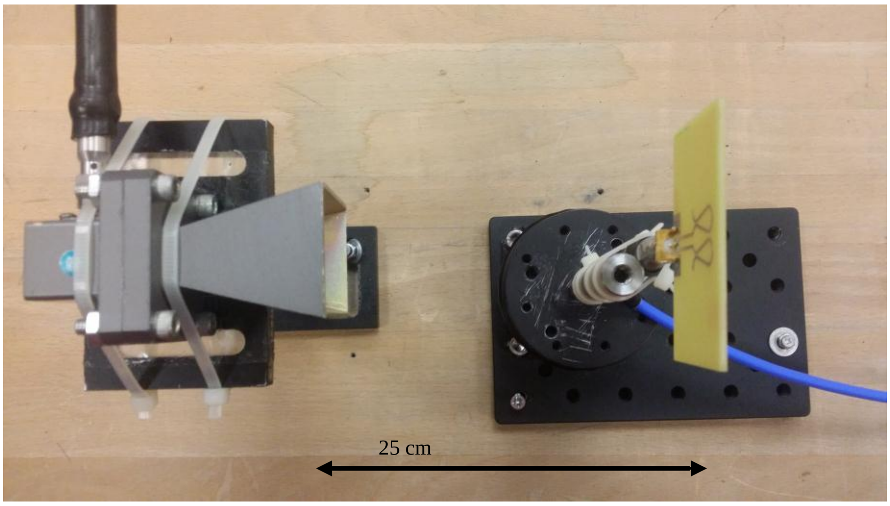

Figure 5.3: Radiation pattern measurement using horn antenna.

Radiation Pattern is measured using a narrow beam horn antenna as shown in Figure 5.3. Antenna under test (AUT) is placed at a distance from receiving antenna to ensure the far field region (25 cm). The pattern was obtained for both elevation and azimuth plane of the antenna. The antenna is mounted on a rotatable mast and radiation pattern is measured a function of angle. The resolution obtained is with the step of 30 degrees for entire 360 degrees measured for both perpendicular and horizontal plane.

Figure 5.4: Agilent HP8719ES Network Analyzer (0.05-13.5GHz).

5.3 Fabricated Designs

In the next section the measurement results of individual is discussed.

5.3.1 Two meandering loops antenna

The first design is 62 mm*40 mm*1.6 mm of physical dimensions with 2 meandering loops. S11 parameters are show in Figure 5.5. Less than -10 dB return loss is observed for the range from 7.96 GHz to 11.03 GHz (3.07 GHz BW). In conformance with the simulation results a dip is observed at 9.5 GHz (-15 dB). The lowest return loss is observed at 8.10 GHz.

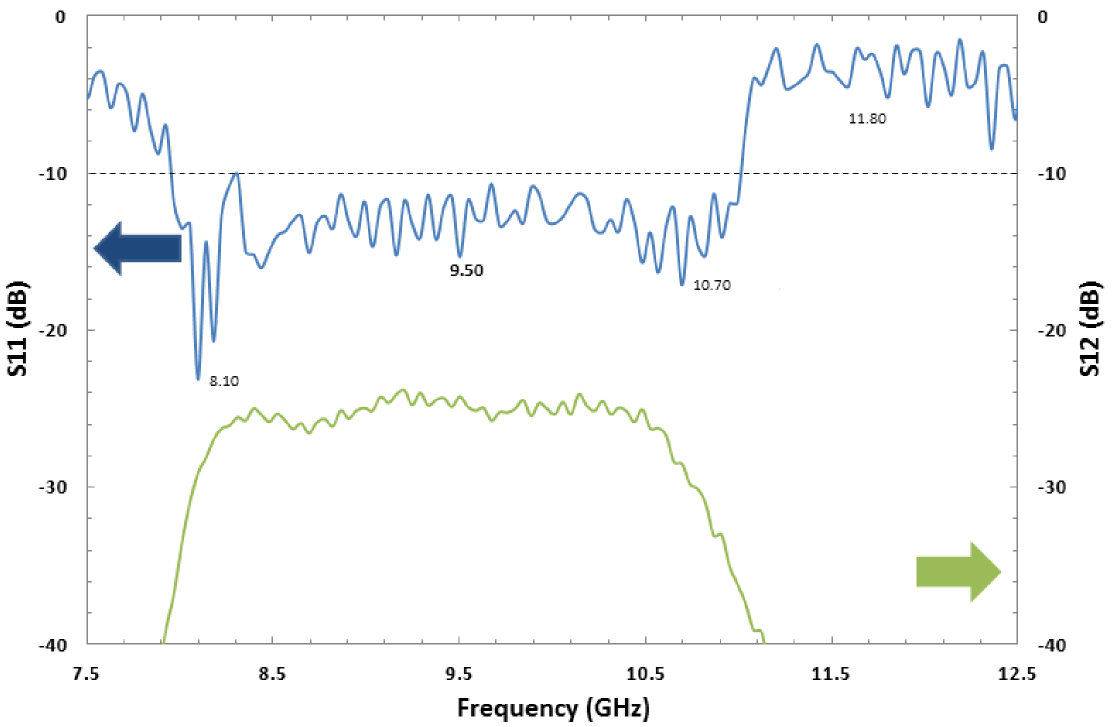

Figure 5.5: Return loss for design one with two meander loops.

Voltage standing wave ratio (VSWR) is < 2 for the bandwidth from 7.96 GHz to 11.03 GHz as shown in Figure 5.6.

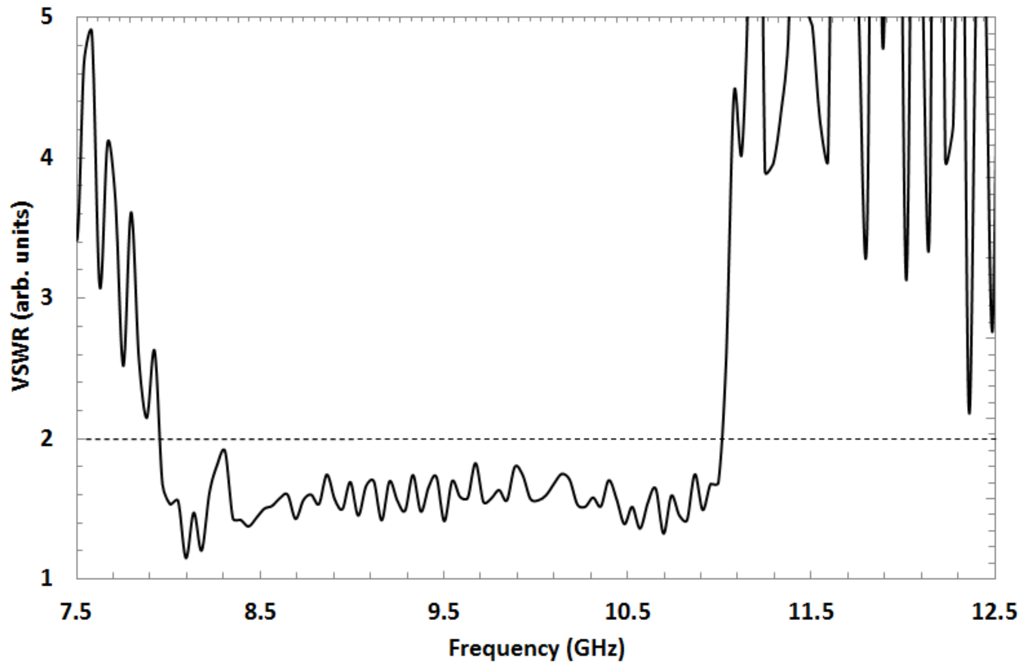

Figure 5.6: Measurement results for VSWR.

The radiation pattern for elevation plane and azimuth field are recorded and shown in Figure 5.7. The radiation pattern is nearly omnidirectional with nulls observed at the feeding points.

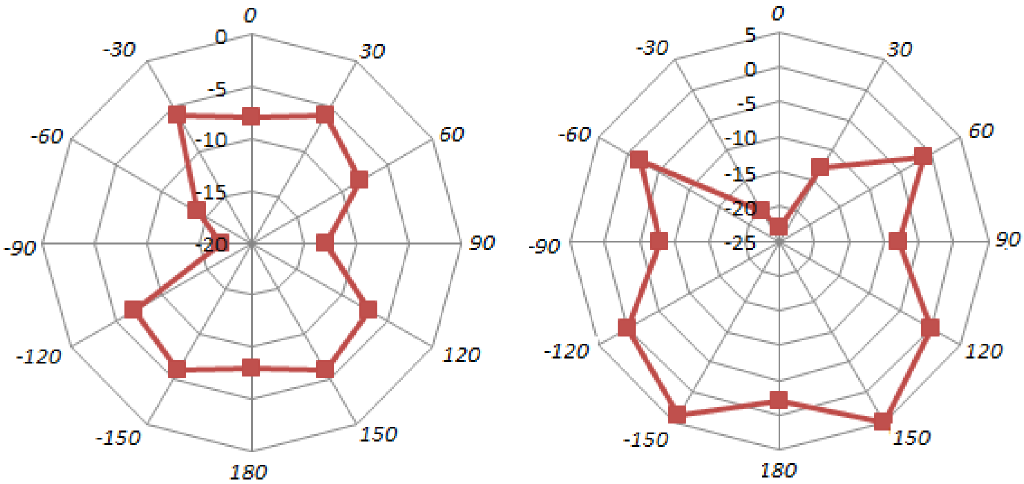

Figure 5.7: 2D radiation pattern for (a) elevation plane (b) azimuth plane .

5.3.2 Four meandering loops antenna

The second design is 62 mm*40 mm*1.6 mm of physical dimensions with 4 meandering loop geometry. S11 and S12 parameters are shown in Figure 5.8. Less than -10 dB return loss is observed for the range from 7.7 GHz to 12.8 GHz (5.1 GHz BW). The lowest value of return loss corresponds to 12.4 GHz.

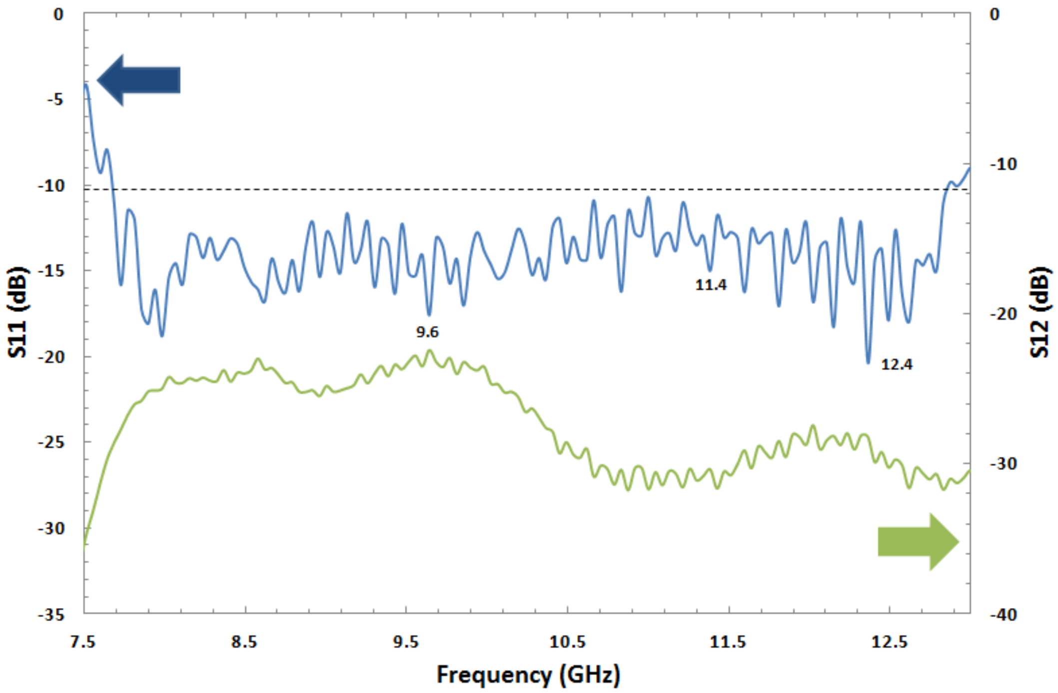

Figure 5.8: Return loss for design with four meander loops

Voltage standing wave ratio (VSWR) is < 2 for the bandwidth from 7.7 GHz to 12.8 GHz as shown in Figure 5.9.

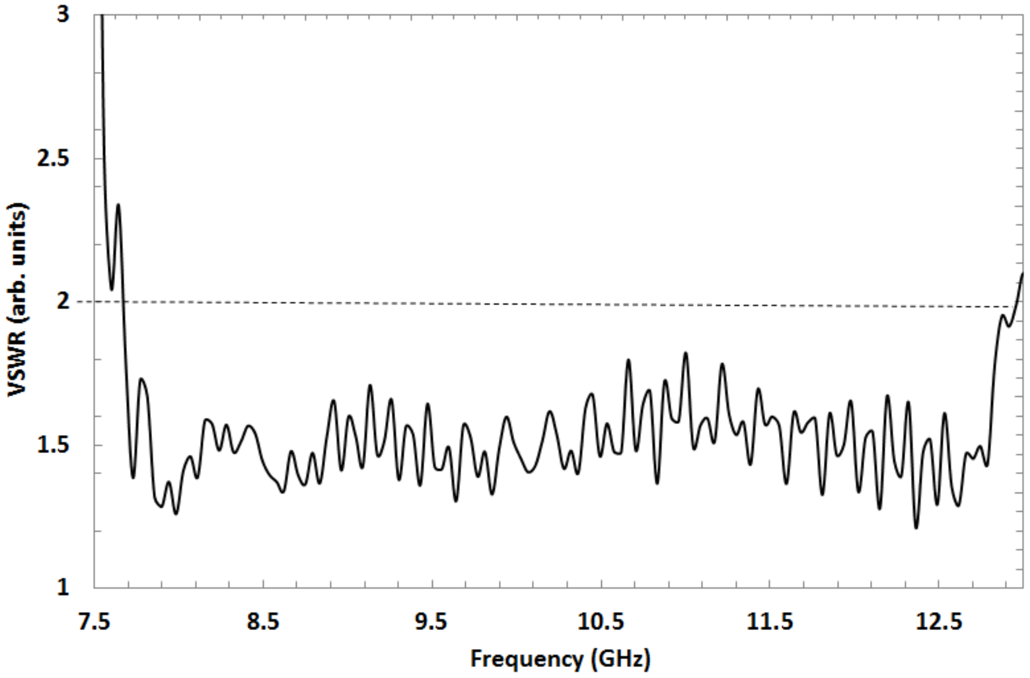

Figure 5.9: Measurement results for VSWR

The radiation pattern elevation and azimuth plane is recorded as shown in Figure 5.10. The nulls are observed at the feeding points.

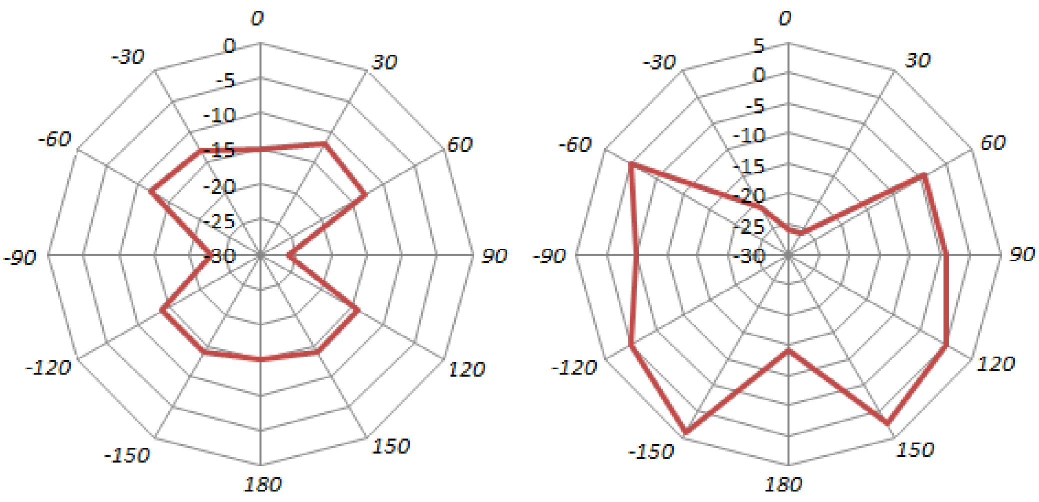

Figure 5.10: 2D Radiation pattern for (a) elevation plane and (b) azimuth plane.

5.3.3 Six meandering loops antenna

The third design is 62 mm*40 mm*1.6 mm of physical dimensions and 6 meanders loop geometry. S11 parameters are show in Figure 5.11. Less than -10 dB return loss is observed for three different ranges, 7.3-8.3GHz, 9.0-9.8GHz and 12.3 - 13 GHz (1GHz, 0.8 GHz, 0.7 GHz BW). The lowest value of return loss corresponds to 7.6 GHz.

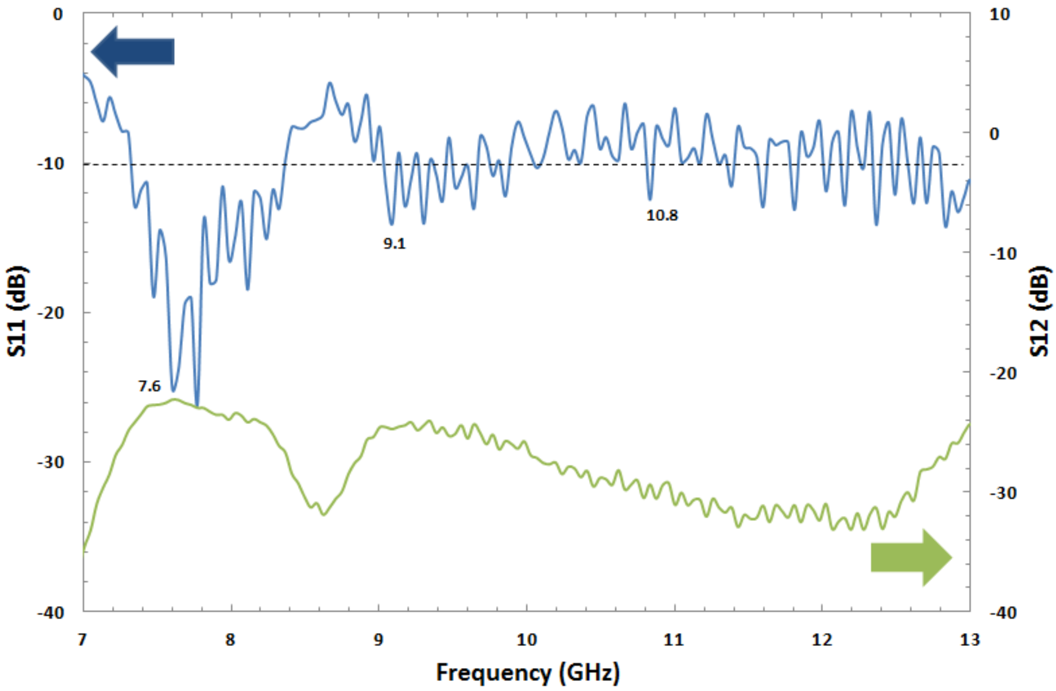

Figure 5.11: Return loss for antenna design with six meander loops.

Voltage standing wave ratio (VSWR) is < 2 for 7.3-8.3GHz, 9.0-9.8 and 12.3 to 13 GHz as shown in Figure 5.12.

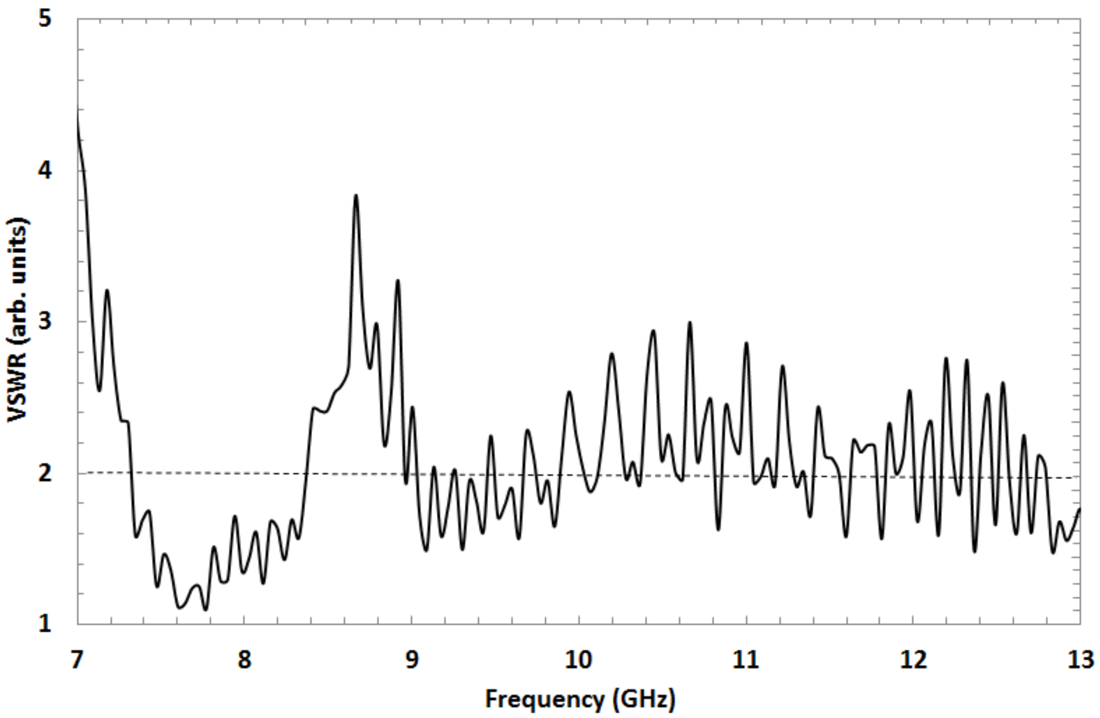

Figure 5.12: Measurement results for VSWR.

The radiation pattern elevation and azimuth plane is recorded and shown in Figure 5.13. The nulls are observed at the feeding points.

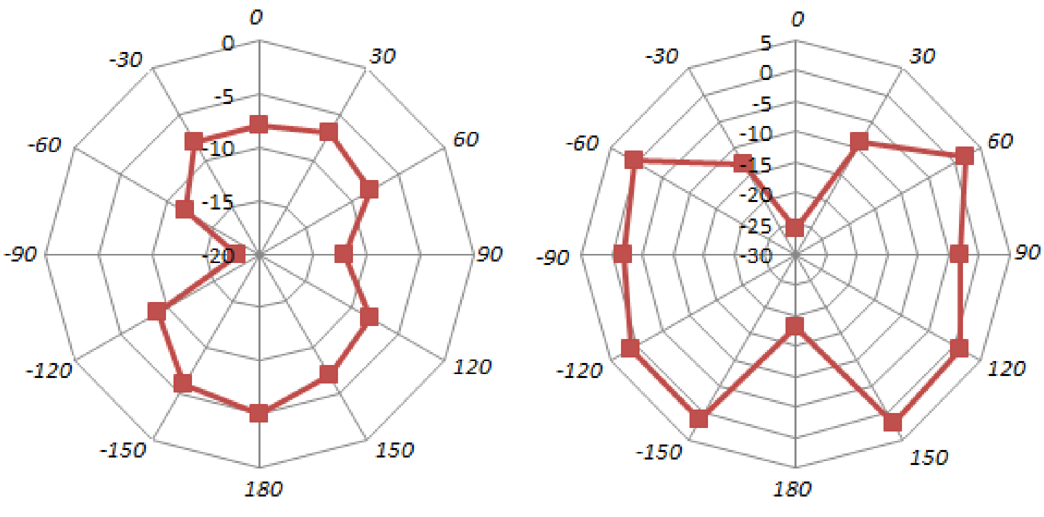

Figure 5.13: 2D Radiation pattern for (a) elevation plane and (b) azimuth plane.

5.3.4 Eight meandering loops antenna

The fourth design is 62 mm*40 mm*1.6 mm of physical dimensions and 8 meanders loop geometry. Both S11 and S12 parameters are show in Figure 5.14. Less than -10 dB return loss is observed for two ranges from 7.85 GHz to 8.3 GHz (0.45 GHz BW) and 11.7 to 13.5 GHz. The best return loss is observed for 8.1 GHz and it is in perfect agreement with the simulated results.

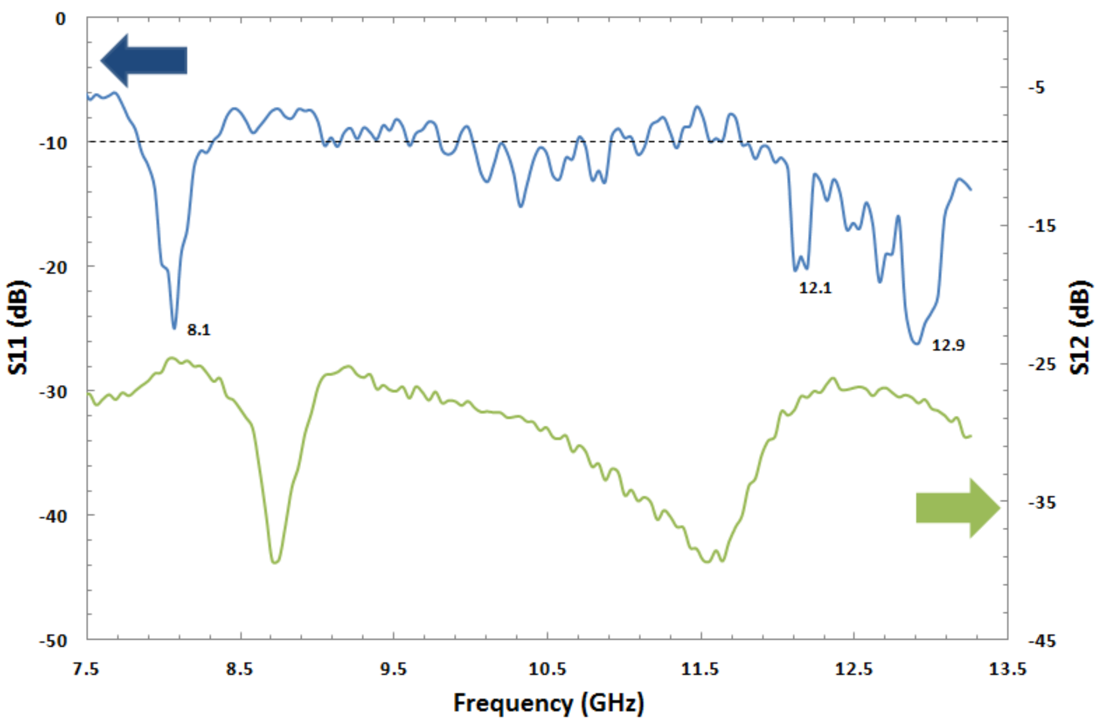

Figure 5.14: Return loss for design with eight meander loops.

Voltage standing wave ratio (VSWR) is < 2 for the bandwidth from 7.8 GHz to 8.3 and 11.7 to 13.5 GHz as shown in Figure 5.15.

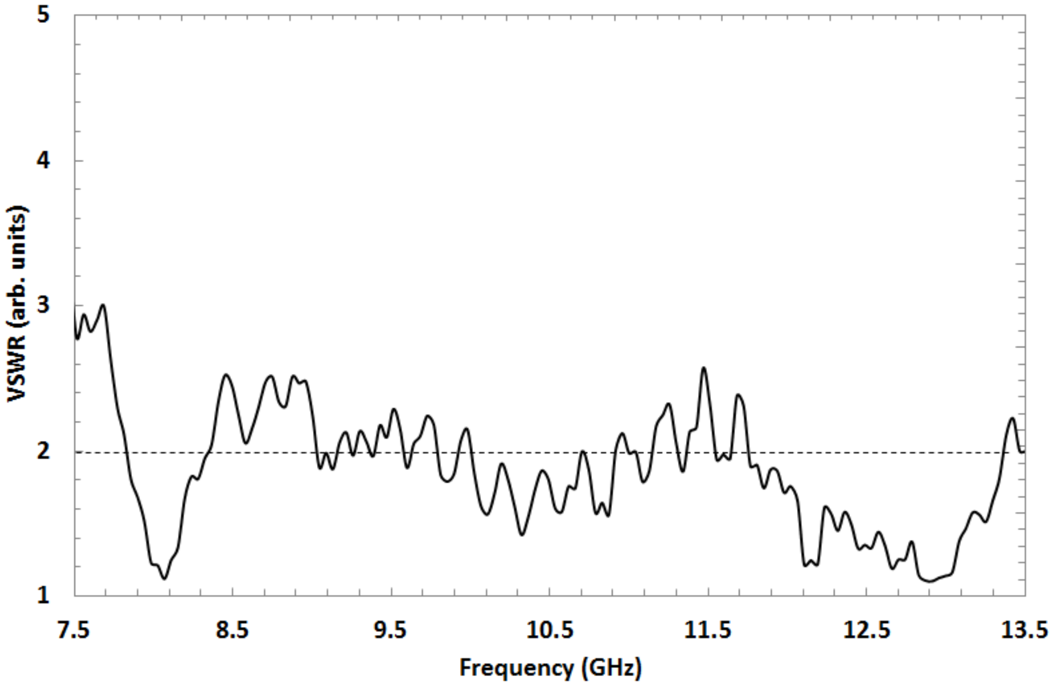

Figure 5.15: Measurement results for VSWR.

The radiation pattern for elevation and azimuth plane is recorded and shown in Figure 5.16. The nulls are observed at the feeding points.

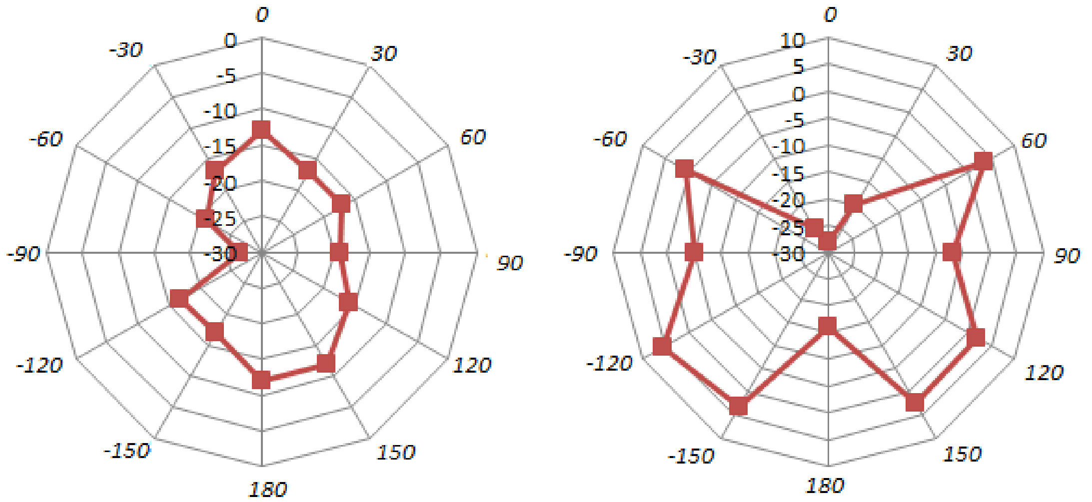

Figure 5.16: 2D Radiation pattern with (a) elevation plane and (b) azimuth plane.

5.3.5 Ten meandering loops antenna

The fifth design is 62 mm*40 mm*1.6 mm of physical dimensions and 10 meandering loops. S11 and S12 parameters are show in Figure 5.17. Less than -10 dB return loss is observed for the range from 6.6 GHz to 7.9 GHz (1.3 GHz BW). The lowest value of return loss corresponds to 6.9 GHz. The transmission peak is observed at the resonance frequency of 9.2 GHz; however due to high mismatch losses at this frequency BW is compromised.

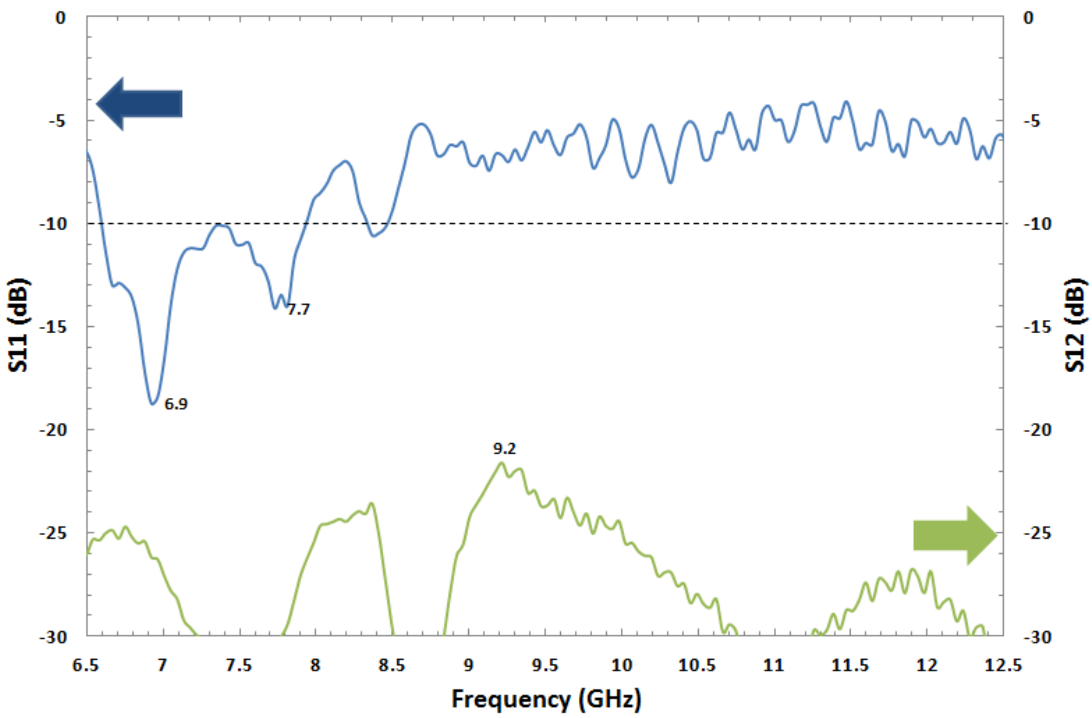

Figure 5.17: Return loss for antenna design with ten meander loops.

Voltage standing wave ratio (VSWR) is < 2 for the bandwidth from 6.6 GHz to 7.9 GHz as shown in Figure 5.18.

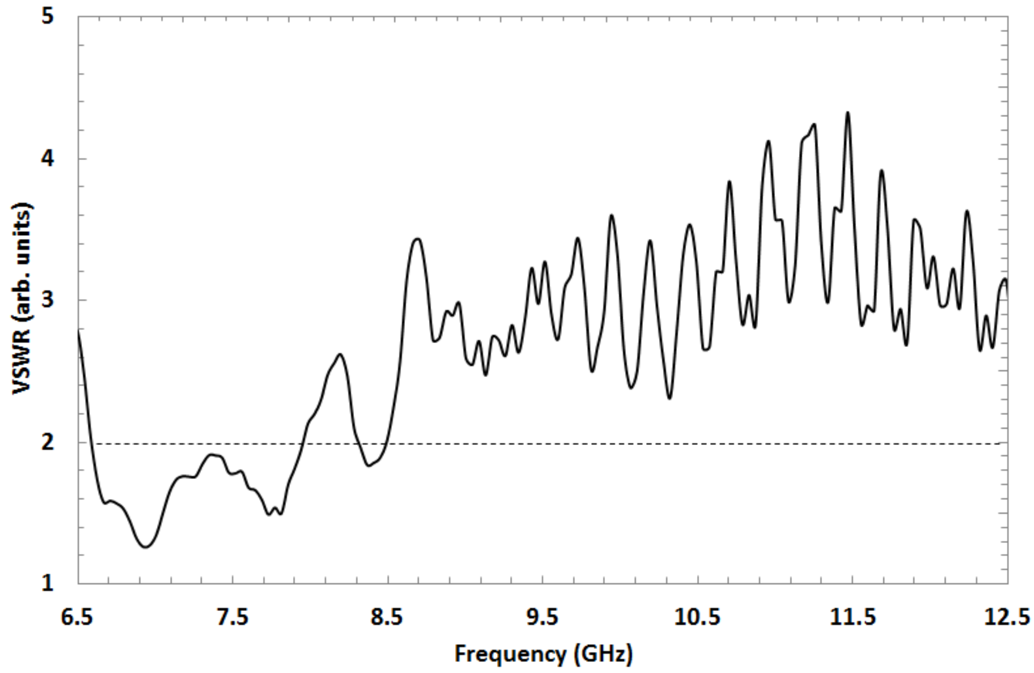

Figure 5.18: Measurement results for VSWR.

The radiation pattern for elevation and azimuth plane is recorded and shown in Figure 5.19. The nulls are observed at the feeding points.

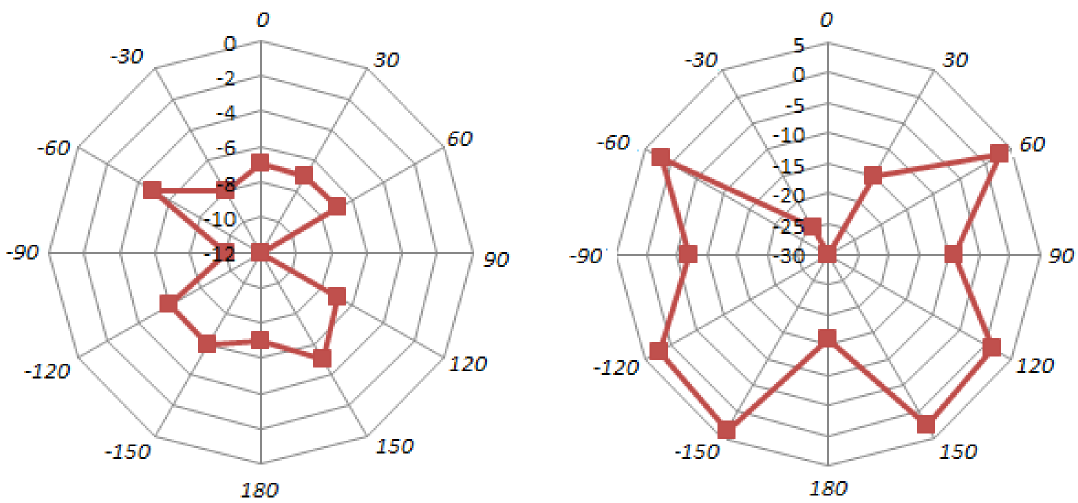

Figure 5.19: 2D radiation pattern with (a) elevation plane and (b) azimuth plane.

5.3.6 Twelve meandering loops antenna

The sixth design is 62 mm*40 mm*1.6 mm of physical dimensions with 12 meandering loops. S11 and S12 parameters are show in Figure 5.20. Less than -10 dB return loss is observed for the range from 7.2 GHz to 8.8 GHz (1.6 GHz BW). The lowest value of return loss corresponds to 7.6 GHz.

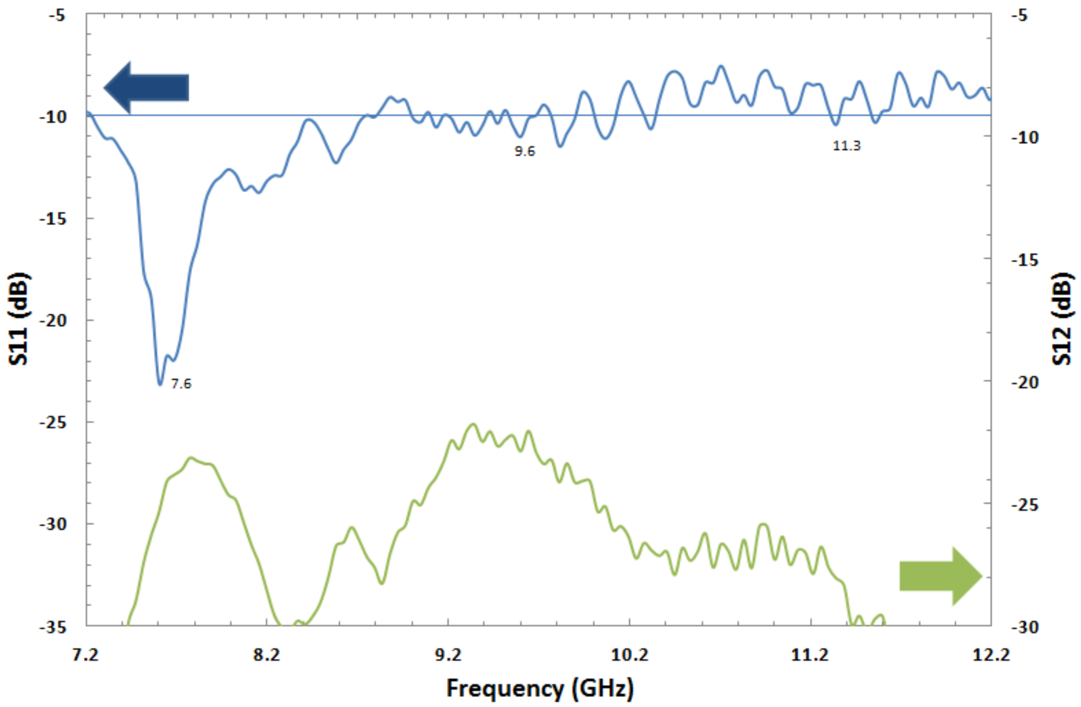

Figure 5.20: Return loss for antenna design with twelve meander loops.

Voltage standing wave ratio (VSWR) is < 2 for the bandwidth from 7.2 GHz to 8.8 GHz as shown in Figure 5.21.

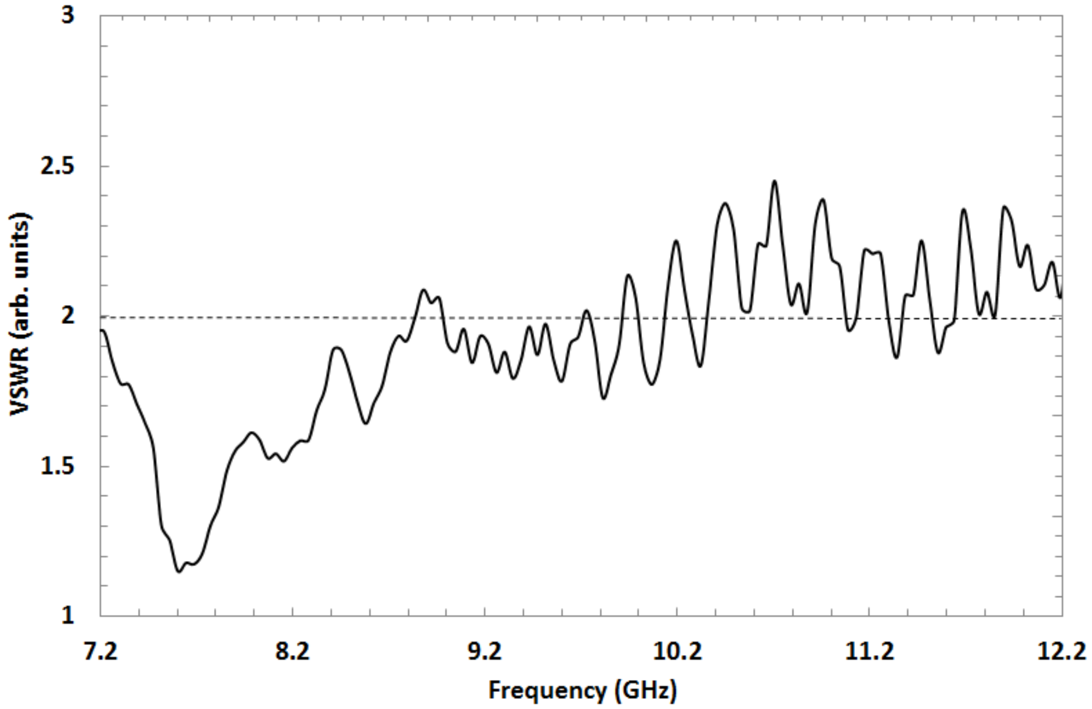

Figure 5.21: Measurement results for VSWR.

The radiation pattern for azimuth and elevation plane is recorded and shown in Figure 5.22. The nulls are observed at the feeding points.

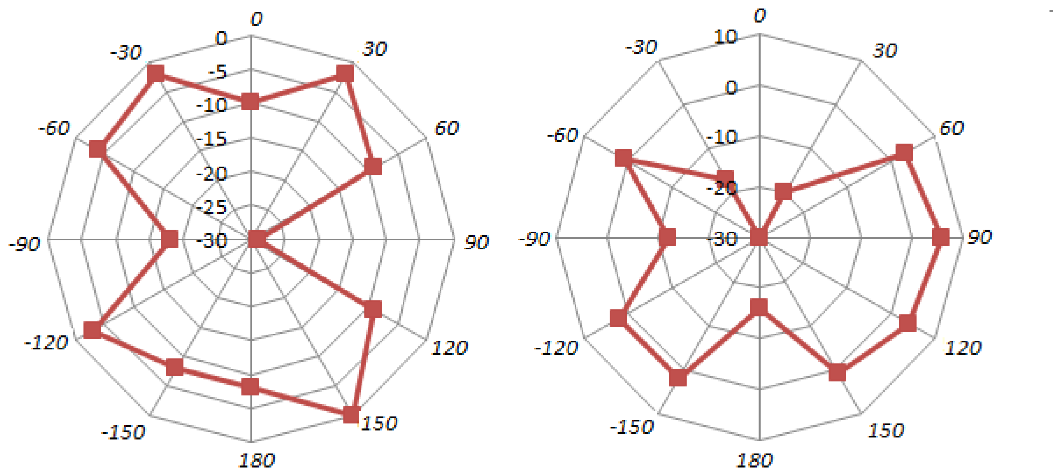

Figure 5.22: 2D Radiation pattern with (a) elevation plane and (b) azimuth plane.

5.4 Summary

The measurement results are summarized in Table 5.1. All designs have promising broad band response and results reflect that they have the ability to radiate in X band. Two meandering loop antennas has a promising 3 GHz response however the spectrum is shifted towards lower frequency response by 1 GHz. The resonance peaks are shifter by 0.4 and 1.1 GHz accordingly. The second design with 4 meandering loops has start band shifted further to the lower frequency response. A shift of 0.4 GHz is observed from the simulated results. These two designs show results closer to the simulated results each with a broadband spectral response and low return loss. Design three with six meandering loops has a resonant shift of 0.4 GHz but BW is limited due to poor impedance matching. Similar anomaly is observed for design four with eight meandering loops. The shift from resonant frequency is 0.7 GHz and high mismatch is observed. Worst case efficiency is measured for design five with ten meandering loops. A shift of 0.5 and 1.1 GHz is observed from the estimated results. Two resonant peaks are in agreement with calculations for design six with twelve meandering loops. The mismatches are higher for this design as well. The deviation from the expected results is attributed to the fabrication anomaly. The coupling distance of 75 microns is not conformal with the fabricated results. It is rather 3 times the actual value. Secondly, The PCB is fabricated using hot air solder leveling (HASL). In HASL, the model is dipped into a bath of molten solder so that all exposed copper surfaces are covered by solder. This technique is absolutely counterproductive for antennas fabrication. It changes the thickness of the conductor (1 Oz for design) and results in impedance mismatch. Thirdly, only design two and design six were fabricated initially, and rest of the designs was obtained by etching away the copper lines. This also contributed to deviation from the calculated and simulated results.

S. No	**No of meanders**	**Start frequency**	**Stop frequency**	**BW**	**Resonating Frequency (f_o)**	**Reflection Loss**	**Gain**	**Efficiency**
-	-	**GHz**	**GHz**	**GHz**	**GHz**	-	**dB**	-
1	2	7.96	11.03	3.07	8.1, 9.5, 10.7	0.22	2.1	0.78
2	4	7.7	12.8	4.1	8.1,9.6, 11.4,12.4	0.18	1.83	0.82
3	6	7.3 9.0 12.3	8.3 9.8 13	1.0 0.8 0.7	7.6, 9.1, 10.8	0.39	3.0	0.61
4	8	7.85 11.7	8.3 13.5	0.45 1.8	8.1, 12.1, 12.9	0.30	1.93	0.70
5	10	6.6	7.9	1.3	6.9, 7.7, 9.2	0.45	1.91	0.55
6	12	7.2	8.8	4.15	7.6, 9.6, 11.3	0.3	1.81	0.70

Table 5.1: Meandering loops in relation to BW, *f*o, RL, efficiency and gain.

6 CONCLUSION

The thesis introduces a new class of meandering loops for broadband microwaves, and photonics passive circuits' applications. Six different antennas are designed in this work and comparison is established on the basis of number of meandering loops. The effect of meandering loops on BW, radiation efficiency, and radiation pattern are studied.

All designs have promising broad band response and results reflect that they have the ability to radiate in X-band. Two meandering loop antennas have a promising 3 GHz response, however the spectrum is shifted towards lower frequency response by 1 GHz. The resonance peaks are shifted by 0.4 and 1.1 GHz, accordingly. The second design with 4 meandering loops has start band shifted further to the lower frequency response. A shift of 0.4 GHz is observed from the simulated results. These two designs show results closer to the simulated results each with a broadband spectral response and low return loss. Design three with six meandering loops has a resonant shift of 0.4 GHz, but the BW is limited due to poor impedance matching. Similar anomaly is observed for design four with eight meandering loops. The shift from resonant frequency is 0.7 GHz and high mismatch is observed. Worst case efficiency is measured for design five with ten meandering loops. A shift of 0.5 and 1.1 GHz is observed from the estimated results. Two resonant peaks are in agreement with calculations for design six with twelve meandering loops. The mismatches are higher for this design as well.

Nearly all antennas have Omni-directional radiation pattern for both simulated and measured results. The nulls were observed mainly around the feeding probes.

All antennas were fabricated using FR4 substrate with standard thickness of 1.6 mm which is significantly cheaper and widely available. Antennas were fabricated on a single sided PCB using a coplanar waveguide (CPW) feed. The main idea was to reduce fabrication time and cost. The overall performance of the antennas was good in terms of, efficiency and return loss.

The antennas with higher order of meandering loops did not show results as expected. The deviation from the expected results is attributed to the fabrication anomaly. The coupling distance of 75 microns is not conformal with the fabricated results of 200 microns. It is rather 3 times the actual value. Secondly, The PCB is fabricated using hot air solder leveling (HASL). In HASL, the model is dipped into a bath of molten solder so that all exposed copper surfaces are covered by solder. This technique is absolutely counterproductive for antennas fabrication. It changes the thickness of the conductor (1 Oz for design) and results in impedance mismatch. It is imperative to elaborate that only design two and design six were fabricated initially, and rest of the designs was obtained by cutting away the copper lines. This also contributed to deviation from the calculated and simulated results. Maximum error of 7 % and 14 % is observed for simulated and measured results.

It is recommended that antennas may be measured in anechoic chamber facility. It could not be carried out due to non-availability at the university. The return losses for the higher meandering loops can be substantially reduced by introducing matching techniques.

We conclude that assigned objective was successfully accomplished. A novel meandering antenna design is introduced as a potential candidate for broadband applications. This novel geometry might open new design platform for microwaves, and photonics passive circuits.

VITA

Muhammad Sohail Anwar was born in Pakistan. He finished high school in 2002. He then had his BE in Aeronautical Engineering from National University of Sciences and Technology (NUST) in 2007.

He then worked in industry over 6 years mainly on microwaves and RF front ends.

In 2013, he received MS scholarship and joined Koç University, Istanbul in M.Sc. Optoelectronics and Photonics Engineering program. He worked at Koç University Microphotonics Research Laboratory.

REFERENCES

1. R. L. Yadava, "Antenna and Wave Propagation," PHI learning private limited, 236 (2011).

2. M. Kay and A. Crosswell, "W2AEE Antenna History," University of Columbia.

3. IEEE Standard Definitions of Terms for Antennas, 1 – 31 (1983).

4. J.P. Carmo , P.M. Mendes, C. Couto and J.H. Correia, " 5.7 GHz on-chip antenna/RF CMOS transceiver for wireless sensor networks'', Sensors and Actuators, Vol 132, 47–51 (2006).

5. W. L. Stutzman, "Estimating Directivity and Gain of Antennas," IEEE Antennas and Propagation Magazine, Vol. 40, 7-11 (1998).

6. D. K. C. Chew and S. R. Saunders, " Meander line technique for size reduction of quadrifilar helix antenna'', IEEE Antennas And Wireless Propagation Letters, Vol. 1, 109-111 (2002).

7. M. Ma and K. Deng , "The Study And Implementation Of Meander Line Antenna For An Integrated Transceiver Design'', MS Thesis Electronics/Telecommunications, University of GAVLE, 2-5 (2010).

8. Y. Bayram, Y. Zhou, B. S. Shim, S. Xu, J. Zhu, N. A. Kotov, and J. L. Volakis, "E-Textile Conductors and Polymer Composites for Conformal Lightweight Antennas''IEEE Transactions on Antennas and Propagation, Vol. 58, 2732 -2736 (2010).

9. M. F. Abedin and M. Ali, “Modifying the ground plane and its effect on planar inverted-F antennas (PIFAs) for mobile phone handsets’’ IEEE Antennas and Wıreless Propagatıon Letters, Vol. 2, 226-229 (2003).

10. C.C. Lin, S.W. Kuo and H.R. Chuang, “A 2.4-GHz printed meander-line antenna for USB WLAN with notebook-PC housing’’, IEEE Microwave and Wireless Components Letters, Vol. 15, 546-549 (2005).

11. H.D. Wu and F. S. Barnes, “Doped $Ba_{0.6}Sr_{0.4}TiO_3$ thin films for microwave device applications at room temperature’’, Integrated Ferroelectrics, Vol 22, 291-305, (1998).

12. M. Miao, B. L. Ooi and P. S. Kooi, “ Broadband CPW-fed wide slot antenna’’ Microwave and Optical Technology Letters, Vol 25, 206–211, (2000).

13. M. Z. Win and R. A. Scholtz, “Ultra-Wide Bandwidth Time-Hopping Spread-Spectrum Impulse Radio for Wireless Multiple Access Communications’’, IEEE Transactions on Communications, Vol. 48, 679-691 (2000).

14. H. Elsadek , “Mobile and Wireless Communications Network Layer and Circuit Level Design", Chapter 9, 163-189 (2010).

15. P. Withington, H. Fluhler, and S. Nag, "Enhancing homeland security with advanced UWB sensors " IEEE Microwave Magazine, Vol 4, 51-58, (2003).

16. D. H. Kwon and D. H. Werner, “Restoration of antenna parameters in scattering environments using electromagnetic cloaking’’ Appl. Phys. Lett. Vol 92, 113507, (2008).

17. P. Kyritsi, D. C. Cox, R. A. Valenzuela and Peter W. Wolniansky, “Effect of antenna polarization on the capacity of a multiple element system in an indoor environment’’, IEEE Journal on Selected Areas in Communications, Vol. 20, 1227-1236, (2002).

18. D.P. Stapor, “Optimal receive antenna polarization in the presence of interference and noise’’, IEEE Transactıons on Antennas and Propagation, Vol. 43, 473-477 (1995).

19. R.L Howard, L.E. Corey, S.P. Williams, “The relationship between dispersion loss, sidelobe levels, and bandwidth in wideband radars with subarrayed antennas’’, IEEE, Antennas and Propagation Society International Symposium, 184-187 (1988).

20. E. R. Brown, C. D. Parker, and E. Yablonovitch, “Radiation properties of a planar antenna on a photonic-crystal substrate’’, Vol. 10, 404-407 (1993).

21. A.C. Polycarpou, P.A. Tirkas, C.A Balanis , “The finite-element method for modeling circuits and interconnects for electronic packaging’’, IEEE Transactıons on Microwave Theory and Techniques, Vol. 45, 1868-1874 (1997).

22. D. Jiawei, L.Y. Xiang and Z. Biao, “A Survey on Radiation Pattern Reconfigurable Antennas’’, 7th International Conference on Wireless Communications, Networking and Mobile Computing (WiCOM), 1-4 (2011).

23. S.V. Parekh, “Simple formulae for circular-polarization axial-ratio calculations’’, IEEE Antenna and propagation magazine, Vol 2, 30-31 (1991).

24. A.C.Polycarpou, P.A. Tirkas, C.A. Balanis, “The finite-element method for modeling circuits and interconnects for electronic packaging’’, IEEE Transactions on Microwave Theory and Techniques, Vol. 45, 1868-1874 (1997).

25. R. Waterhouse, “Printed Antennas for Wireless Communications”, Sussex, England: John Wiley and Sons Ltd, 183-184, (2007).

26. K. Fujimoto, “Mobile Antenna Systems Handbook’’, 3rd Edition, 606-609, (2006).

27. M. H. Al Sharkawy, A.A. Eldek, A. Z. Elsherbeni and C. E. Smith, "Design of Wideband Printed Monopole Antenna Using WIPL-D, 20th Annual Review of Progress in Applied Computational Electromagnetics, Vol 15, 1-5 (2004).

28. K. Fujimoto, A. Henderson, K. Hirasawa, and J. R. James, "Small Antennas," Research Studies Press, England, 9th Edition (1993).

29. K. P. Ray, "Design Aspects of Printed Monopole Antennas for Ultra-Wide Band Applications", International Journal of Antennas and Propagation Vol 8, 1-8 (2008).

30. S. I. Latif, L. Shafai, and S. K. Sharma, "Bandwidth enhancement and size reduction of microstrip slot antenna," IEEE Trans. Antennas Propag., vol. 53, 994-1003 (2005).

31. R. N. Simons and R. Q. Lee, “ Coplanar Waveguide Feeds for Phased Array Antennas’’, NASA Technical Memorandum 104467 AIAA-91-3422, 1-8 (1991).

32. M. Keskilammi, L. Sydänheimo and M. Kivikoski, " Passive RFID Systems and the Effects of Antenna Parameters on Operational Distance'', International Journal of Advanced Manufacturing Technology, Vol 21, 769-774 (2003).

33. http://wcalc.sourceforge.net/cgi-wcalc.html

34. C.A. Balanis. "Antenna Theory Analysis and Design" New York: John Wiley&Sons Ltd. pp.1, 28, 723 (1997).

35. P. H. Cole, L. Zhang, " A Method for Calculating the Resonant Frequency of Meander-line Dipole Antenna, IEEE Industrial Electronics and Applications (ICIEA) Conference, Vol 09, 1783-1786 (2009).